December 1996

Oversampling PCM techniques and optimum noise shapers for quantizing a class of nonbandlimited signals

Jamal Tuqan and P. P. Vaidyanathan
Department of Electrical Engineering

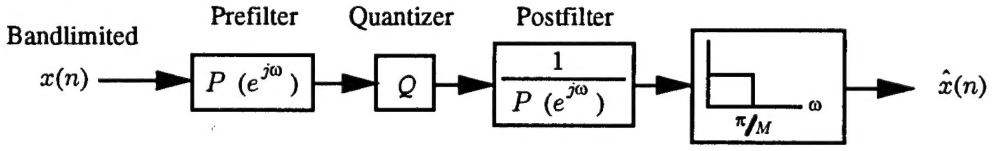

Schematic of the traditional oversampling PCM technique with noise shapers

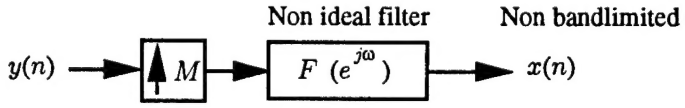

The single band model

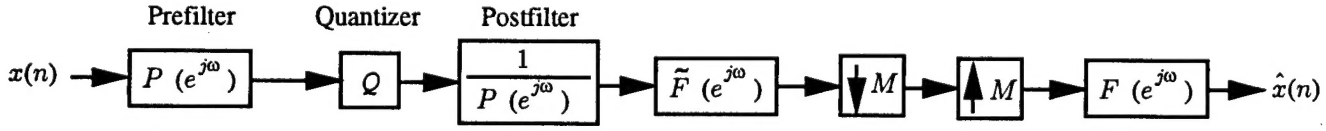

Schematic of the new quantization scheme for the single band model using a model matched multirate low pass filter

California Institute of Technology

Pasadena, CA 91125

OVERSAMPLING PCM TECHNIQUES AND OPTIMUM NOISE SHAPERS FOR QUANTIZING A CLASS OF NONBANDLIMITED SIGNALS ‡

Jamal Tuqan, Student member, IEEE and P.P. Vaidyanathan, Fellow, IEEE

Department of Electrical Engineering 136-93

California Institute of Technology

Pasadena, CA 91125, USA.

Phone: (818) 395-4681 Fax: (818) 795-8649

Contact author: P. P. Vaidyanathan, E-mail : ppvnath@sys.caltech.edu

Abstract. We consider the quantization of a class of *non bandlimited* signals, namely the class of discrete time signals that can be recovered from their decimated version. Based on recent results, the signals of interest are assumed to be the output of a single interpolation filter (single band model) or more generally the sum of the outputs of L interpolation filters (multiband model). By definition, these signals are oversampled and it is reasonable to expect that we can reap the same benefits of well known efficient A/D techniques. In fact, by using appropriate multirate models and reconstruction schemes, we first show that we can obtain a great reduction in the quantization noise variance due to the oversampled nature of the signals. Alternatively, we also show that we can achieve a substantial decrease in bit rate by appropriately decimating the signals and then quantizing them. To further increase the effective quantizer resolution, noise shaping is introduced by optimizing pre- and post filters around the quantizer. We start with a scalar time invariant quantizer and study two important cases of LTI filters, namely the case where the postfilter is the inverse of the prefilter and the more general case where the postfilter is not related to the prefilter. Closed form expressions for the optimum filters and minimum mean squared error are derived in each case for both the single band and multiband models. Due to the statistical nature of the signal of interest, the class of noise shaping filters and quantizers is then enlarged to include linear periodically time varying $(LPTV)_M$ filters and periodically time varying quantizers of period M. Because the general $(LPTV)_M$ case is difficult to track analytically, we study two special cases in great detail and give complete solutions for both the single band and multiband models. Examples are also provided for performance comparisons between the LTI case and the corresponding $(LPTV)_M$ one.

‡ Work supported in parts by Office of Naval Research grant N00014-93-1-0231, Tektronix, Inc., and Rockwell International.

I. INTRODUCTION

It is well known that if a continuous time signal $x(t)$ is σ-bandlimited, then, it can be recovered uniquely from its samples $x(nT)$ as long as $T \leq \pi/\sigma$. Extensions of the lowpass sampling theorem such as the bandpass, non uniform and derivative sampling theorems can be found in [1]. Recently, Walter [2] showed that, under some conditions, a class of non bandlimited continuous time signals can be reconstructed from uniformly spaced samples even though aliasing occurs. Vaidyanathan and Phoong [3], [4] developed the discrete time version of Walter's result from a multirate digital filtering perspective. In specific, they considered the class of non bandlimited signals that can be modeled as the output of a single interpolation filter (single band model) as in Fig. 1 or as the output of the more general multiband model of Fig. 2. The filter $F(e^{j\omega})$ in Fig. 1 and the filters $F_k(e^{j\omega})$, $k = 0, 1, \ldots, L-1$, in Fig. 2 are usually a subset of L synthesis filters in an M channel maximally decimated perfect reconstruction filter bank, although this is not a necessary condition. To give the reader a flavor of the major ideas, consider for the moment the single band model of Fig. 1. The discrete time signal $x(n)$ is the output of an interpolation filter $F(e^{j\omega})$. Even though this signal is not in general bandlimited, it is natural to expect that it can be recovered from its decimated version $x(Mn)$. To see this, assume that $x(n)$ is modeled as in Fig. 1 and consider $x(Mn)$, the M-fold decimated versions of $x(n)$. If $F(e^{j\omega})$ is a Nyquist(M) filter [5], then, $x(Mn)$ is equal to $y(n)$ and we have the relation $x(n) = \sum_k x(kM) f(n - kM)$. In other words, $x(n)$ is completely defined by the samples $x(Mn)$ even though the filter $F(e^{j\omega})$ is not necessarily ideal. In [4], the authors consider the case where $F(e^{j\omega})$ is not necessarily a Nyquist(M) filter and show how similar reconstruction can be done. They also consider the stability of the reconstruction process. It turns out that if one of the polyphase components of $F(e^{j\omega})$ is free from unit circle zeros, then, stability of reconstruction is guaranteed. Furthermore, even if all the polyphase components of $F(e^{j\omega})$ have unit circle zeros, stable reconstruction can still be achieved by using non uniform decimation. In this case, a sufficient condition for stable reconstruction is that $F(e^{j\omega})$ (assumed FIR) has two polyphase components with no multiple zeros, i.e., each polyphase component has distinct zeros and they do not share any common zero.

In this paper, we consider the efficient quantization of this class of non band-limited signals that can be modeled as in Fig. 1 or more generally as in Fig. 2. To motivate such a study, consider the schematic shown in Fig. 3 where the box labeled Q is a simple uniform roundoff (PCM) quantizer. After going through the quantizer, the signal $x(n)$ is now contaminated by an additive noise component $e(n)$. Assuming that the signal $x(n)$ is bandlimited or equivalently oversampled (since a bandlimited signal can be further downsampled), we can low pass filter the quantized signal $x(n) + e(n)$. The ideal low pass filter on the right removes the noise in the stopband but does not change the signal component. In terms of signal and noise power, the signal power remains unchanged whereas the noise power decreases proportionally to the oversampling ratio, usually expressed in the form 2^r. It can be shown that for every doubling of the oversampling ratio, i.e., for every unit increment in r, the signal to noise ratio (SNR) improves by about 3 db or equivalently, the quantizer resolution improves by one half bit (see for example [6]). After low-pass filtering, the quantized signal can be downsampled to the Nyquist rate without affecting the signal to noise ratio. The idea is therefore to exploit the oversampled nature of the signal $x(n)$ to

tradeoff quantizer complexity for higher resolution. This technique is usually called oversampled PCM conversion. Consider now the system of Fig. 4 where $P(e^{j\omega})$ is a linear time-invariant (LTI) filter. The input signal $x(n)$ is still assumed to be oversampled (bandlimited). In addition to the benefits described above, it can be shown that this more sophisticated system produces a further decrease in the noise power by "cleverly" choosing the filter $P(e^{j\omega})$ in Fig. 4. The filter pair $P(e^{j\omega})$ and $1/P(e^{j\omega})$ does not modify the input signal $x(n)$ in any way but only affects the noise component $e(n)$. Similar to sigma-delta quantizers, the system of Fig. 4 introduces *noise shaping* in the signal band to allow higher resolution quantization of bandlimited signals.

With these ideas in mind, observe now the output $x(n)$ of Fig. 1. Even though $x(n)$ is not bandlimited, it can be reconstructed from its downsampled version as explained above. In this sense, *it can be considered as an oversampled signal.* The question then arises : Can we obtain advantages similar to the above schemes for a non bandlimited signal satisfying the model of Fig. 1 and more generally of Fig. 2 ? Furthermore, for a fixed set of filters $F(e^{j\omega})$ (or $F_k(e^{j\omega})$, $k = 0, 1, \ldots, L-1,$), what is the best filter prefilter $P(e^{j\omega})$ that minimizes the noise power at the output ? Do we gain more by using a more general postfilter $V(e^{j\omega})$ instead of $\frac{1}{P(e^{j\omega})}$? This is a sample of the type of questions we answer in this paper. Indeed, we will show that, by replacing the ideal low pass filter with the correct multirate reconstruction system, we can reap the same quantization advantages as in the bandlimited case. As a simple example, consider the scheme of Fig. 5 where the finite order filter $F(e^{j\omega})$ is such that its magnitude squared response $|F(e^{j\omega})|^2$ is Nyquist(M), that is, $(|F(e^{j\omega})|^2) \downarrow_M = 1$ (we will motivate such an assumption later in the paper). With this assumption, it can be shown that the signal $\hat{x}(n)$ in Fig. 5 is equal to $x(n)$ in the absence of the quantizer and that the entire scheme of Fig. 5 behaves similarly to Fig. 3, except that the low pass filtering is now *multirate* and *non ideal.* Thus, generally speaking, if a non bandlimited signal can be reconstructed from its samples $x(Mn)$ because it satisfies a model like Fig. 1, then, a low precision quantizer should allow us to produce a high precision version $\hat{x}(n)$.

To bring the analogy closer to the scheme of Fig. 4, we should introduce noise shaping. This can be done by using a pre- and post filter before and after the quantizer respectively as shown in Fig. 6. The prefilter $P(e^{j\omega})$ is traditionally an integrating low pass filter. The post filter $1/P(e^{j\omega})$ shapes the noise spectrum in order to further decrease the noise variance. In this paper, we will derive closed form expressions for the optimal choice of $P(e^{j\omega})$ and the minimum average mean square error obtained from such a scheme. Several extensions to the above noise shaping idea are then introduced. For example, we relax the requirement that the postfilter is the inverse of the prefilter and assume a more general postfilter $V(e^{j\omega})$. Closed form expressions for the optimum filters in this case and the minimum mean squared error are also derived. We would like to warn the reader at this point that no optimization of finite order filters is performed in this paper. The emphasis is actually to find an expression for the theoretically optimum filters (without order constraint) to get an upper bound on the achievable gain with practical inexpensive filters.

The quantization advantage offered by Fig. 5 and Fig. 6 can be useful, for example, in the following realistic engineering scenario. Suppose $x(n)$ is generated at a point where we cannot afford very complex signal processing

(e.g., in deep space) and needs to be transmitted to a distant place (e.g., earth station). If we have the knowledge that $x(n)$ admits a satisfactory model like Fig. 1, we can compress it using a very simple low pass filter $P(e^{j\omega})$ with one or two multipliers and then quantize the output before transmission. The post filter $1/P(e^{j\omega})$ and the expensive multirate filter are at the receiver end, where the complexity is acceptable.

Assume now that the main aim is to obtain a reduction in the bit rate (number of bits per second) rather than accuracy (number of bits per sample). If we are allowed to perform discrete time filtering (of arbitrary complexity), we will see that the best approach would be as in Fig. 7. In this set up, we first generate the driver signal $y(n)$ and then quantize it. The signal $\hat{x}(n)$, which is equal to $x(n)$ in absence of quantization, is then generated. The lower rate signal $y(n)$ in Fig. 7 can be regarded as the principal component signal in an orthonormal subband coder. We will see throughout this paper that, by choosing this type of quantization system, we can obtain a large reduction in the bit rate and/or the quantization accuracy depending on the particular signal model.

Summarizing, the main issue in this paper is how to take advantage of the signal model (Fig. 1 or Fig. 2) in preparing a quantized or compressed version of $x(n)$. Our study is motivated by similar concepts that arises in A/D conversion applications. We find that the choice of a particular scheme depends on how much processing we are allowed to do before quantization. If processing is allowed, we first generate $y(n)$ by filtering and decimation and then quantize it. Otherwise, we quantize $x(n)$ directly and then filter the quantized signal with the appropriate multirate scheme. Noise shaping can be also introduced to obtain better resolution. In any case, an improvement in accuracy and/or bit rate due to the signal model is always achieved.

1.1. Main results and outline of the Paper

1. In section II, definitions and well established facts of various multirate and statistical signal processing concepts used throughout the paper are reviewed.

2. In section III, new results that describe the statistical behavior of signals as they pass through multirate interconnections are presented. These results will then be used to derive the theorems of interest of the paper.

3. In section V, we give several results on the quantization of the non bandlimited signal $x(n)$ modeled as in Fig. 1. The signal $x(n)$ is first quantized to an average of b bits per sample and then filtered by the multirate interconnection in Fig. 5. We show that the multirate system does not affect the signal component but reduces the noise variance by a factor of M. This amounts to the same quantitative advantage obtained from the oversampling PCM technique (0.5 bit reduction per doubling of the oversampling ratio).

4. In section VI, the lower rate signal $y(n)$ is quantized instead of $x(n)$. By quantizing $y(n)$ to b bits per sample, the quantization bit rate (number of bits per second) is decreased by a factor of M but noise reduction due to multirate filtering is now not possible.

5. In section VII, noise shaping is introduced in order to obtain better accuracy. First, we consider the use of pre- and post linear time invariant filters $P(e^{j\omega})$ and $\frac{1}{P(e^{j\omega})}$ as in Fig. 6 together with a fixed time invariant quantizer $\mathcal{Q}$. For this case, the optimum filter $P_{opt}(e^{j\omega})$ that minimizes the quantization noise variance in the reconstructed output $\hat{x}(n)$ is derived and a closed form expression for the average minimum mean square error is obtained. We

then consider the more general pre- and postfilters $P(e^{j\omega})$ and $V(e^{j\omega})$ as in Fig. 8. Closed form expressions for the optimum filters and the average minimum mean square error are also found for this case.

6. In section VIII, we replace the linear time invariant filter $P(e^{j\omega})$ with a more general linear periodically time varying filter of period M. This is motivated by the cyclo-widesense stationarity of $x(n)$. Since the problem of finding the optimum general $(LPTV)_M$ filter (equivalently biorthogonal filter bank) is analytically difficult to track, optimal solutions are given for two special cases of $(LPTV)_M$ filters. The first solution is for the set of M filters $V_k(e^{j\omega})$ shown in Fig. 9. The filters $V_k(e^{j\omega})$ and $\frac{1}{V_k(e^{j\omega})}$ act as pre- and post filters for the kth subband quantizer. The second solution is for the case of an orthonormal filter bank or equivalently for a lossless $(LPTV)_M$ filter. The scheme is shown in Fig. 10 for the single band case.

7. All the results mentioned above are also generalized for the multiband case. Furthermore, examples are provided whenever necessary for illustrative purposes.

II. SUMMARY OF STANDARD MULTIRATE CONCEPTS

1. Notations. Lower case letters are used for scalar time domain sequences. Upper case letters are used for transform domain expressions. Bold faced quantities represent vectors and matrices. The superscripts T, $*$ and $\dagger$ denote respectively the transpose, conjugate and the conjugate transpose operations for vectors and matrices. The M-fold downsampler has an input-output relation $y(n) = x(n)\downarrow_M = x(Mn)$. The M-fold expander's input-output relation is $y(n) = x(n)\uparrow_M = x(n/M)$ when n = multiple of M and $y(n) = 0$ otherwise. The M-fold polyphase representation of $X(e^{j\omega})$ is given by $X(e^{j\omega}) = X_0(e^{jM\omega}) + e^{-j\omega}X_1(e^{jM\omega}) + e^{-j2\omega}X_2(e^{jM\omega}) + \ldots + e^{-j(M-1)\omega}X_{M-1}(e^{jM\omega})$. The polyphase components are given by $x_k(n) = x(Mn+k)$ or, in the frequency domain by $X_k(e^{j\omega}) = (e^{j\omega k}X(e^{j\omega}))\downarrow_M$. The tilde accent on a function $\mathbf{F}(z)$ is defined such that $\tilde{\mathbf{F}}(z)$ is the conjugate transpose of $\mathbf{F}(z)$, i.e., $\tilde{\mathbf{F}}(z) = \mathbf{F}^\dagger(1/z^*)$.

2. Blocking a signal. Given a scalar signal $x(n)$, we define its M-fold blocked version $\mathbf{x}(n)$ by

$$\mathbf{x}(n) = \begin{pmatrix} x(nM) & x(nM-1) & \ldots & x(nM-M+1) \end{pmatrix}^T \tag{1}$$

Equivalently, the scalar sequence $x(n)$ is called the unblocked version of the vector process $\mathbf{x}(n)$. The blocking and unblocking operations are shown in Fig. 11. The elements of the blocked version $\mathbf{x}(n)$ are the polyphase components of $x(n)$.

3. Cyclo-widesense stationary process. A stochastic process $x(n)$ is said to be cyclo-widesense stationary with period M, abbreviated as $(CWSS)_M$, if the M-fold blocked version $\mathbf{x}(n)$ is WSS. Alternatively [7], [8], a process $x(n)$ is $(CWSS)_M$ if the mean and autocorrelation functions of $x(n)$ are periodic with period M, i.e.,

$$E[x(n)] = E[x(n+kM)]\ \forall\ n,k \text{ and } R_{xx}(n,k) = R_{xx}(n+M,k)\ \forall\ n,k. \tag{2}$$

where $R_{xx}(n,k) \triangleq E[x(n)x^*(n-k)]$ is the autocorrelation function of $x(n)$.

4. Antialias(M) filters. $F(e^{j\omega})$ is said to be an antialias(M) filter if its output can be decimated M-fold without aliasing, no matter what the input is. Equivalently, there is no overlap between the plots $F(e^{j(\omega-(2\pi k/M))})$ for distinct k in $0 \le k \le M-1$. Since this requires a stopband with infinite attenuation, these are ideal filters.

5. Orthonormal filter bank. An M-channel maximally decimated uniform filter bank (FB) is said to have the perfect reconstruction (PR) property when $\mathbf{R}(e^{j\omega}) = \mathbf{E}^{-1}(e^{j\omega})$ where $\mathbf{E}(e^{j\omega})$ and $\mathbf{R}(e^{j\omega})$ denote respectively the analysis and synthesis polyphase matrices [8]. In the case of an orthonormal filter bank, the analysis polyphase matrix is paraunitary, i.e., $\mathbf{E}(e^{j\omega})\mathbf{E}^{\dagger}(e^{j\omega}) = \mathbf{I}\ \forall\ \omega$ and we choose $\mathbf{R}(e^{j\omega}) = \mathbf{E}^{\dagger}(e^{j\omega})$ for perfect reconstruction. The analysis and synthesis filters are related by $F_k(e^{j\omega}) = \tilde{H}_k(e^{j\omega})$, that is $f_k(n) = h_k^*(-n)$. It follows that, for an orthonormal filter bank, the energy of each analysis/synthesis filter equals unity, that is $\int_{-\pi}^{\pi} |F_k(e^{j\omega})|^2 \frac{d\omega}{2\pi} = 1$.

6. The coding gain of a system. Assume that we quantize $x(n)$ directly with b bits as shown in Fig. 12. We denote the corresponding mean square error (m.s.e) by $\mathcal{E}_{direct}$. We then use the optimum pre and post filters (in the mean square sense) around the quantizer. With the rate of the quantizer fixed to the same value b, we denote the minimum m.s.e in this case by $\mathcal{E}_{min}$. The ratio $\mathcal{E}_{direct}/\mathcal{E}_{min}$ is called the coding gain of the new system and, as the name suggests, is a measure of the benefits provided by the pre/post filtering operation.

III. PRELIMINARY RESULTS

Result 1. *Consider any L synthesis filters ($L < M$) of an M-channel orthonormal filter bank as shown in Fig. 2. Assume that the L inputs $y_k(n)$ to the synthesis filters $F_k(e^{j\omega})$ are zero mean jointly WSS processes, not necessarily uncorrelated. Then, the statistical correlation (averaged over M samples) between the interpolated subband signal $x_i(n)$ and the M-sample shifted process $x_j(n - Mm)$ is zero, for all values of $i \neq j$ and m, that is:*

$$\frac{1}{M}\sum_{k=0}^{M-1} E[x_i(n-k)x_j{}^*(n-k-Mm)] = 0,\ \forall\ n, m \text{ and } \forall\ i, j \in [0, L-1] \tag{3}$$

The proof can be found in appendix A. As a consequence, the average variance of the $(CWSS)_M$ output process $x(n)$ of Fig. 2, where the filters $F_k(e^{j\omega})$ are any L synthesis filters of an M-channel orthonormal filter bank, is:

$$\sigma_x^2 = \frac{1}{M}\sum_{k=0}^{L-1} \sigma_{y_k}^2 \tag{4}$$

This can be seen by substituting $x(n)$ in the formula $\sigma_x^2 = \frac{1}{M}\sum_{n=0}^{M-1} E[|x(n)|^2]$ and using result 1 for the special case of $m = 0$ and $n = M-1$. If the L inputs to the synthesis filters $F_k(e^{j\omega})$ are zero mean uncorrelated WSS processes, the previous result holds without the orthonormality requirement on the filters $F_k(e^{j\omega})$, $k = 0, 1, \ldots, L-1$.

Result 2. *Consider the multirate interconnection of Fig. 1 where the input $y(n)$ is zero mean WSS random process. If $F(e^{j\omega})$ is a filter (not necessarily ideal) with a Nyquist(M) magnitude squared response, then*

$$\sigma_x^2 = \frac{1}{M}\sigma_y^2 \tag{5}$$

where σ_x^2 is the average variance of the $(CWSS)_M$ output $x(n)$.

Proof. While this is a special case of the above with $L = 1$, the following proof is direct and more instructive. With $F(e^{j\omega})$ expressed in terms of its polyphase components $R_k(e^{j\omega})$, Fig. 1 can be redrawn as in Fig. 13. The

signal $x(n)$ is the interleaved version of the WSS outputs of $R_k(e^{j\omega})$. So, it has zero mean and a variance which is periodic with period M. The average variance is given by :

$$\sigma_x^2 = \frac{1}{M}\sum_{k=0}^{M-1}\sigma^2{}_{x_k} = \frac{1}{M}\int_{-\pi}^{\pi} S_{yy}(e^{j\omega})\sum_{k=0}^{M-1}|R_k(e^{j\omega})|^2\frac{d\omega}{2\pi} \tag{6}$$

The Nyquist property of $|F(e^{j\omega})|^2$ implies in particular that $\sum_{k=0}^{M-1}|R_k(e^{j\omega})|^2 = 1$ (see [5] pp. 159). The preceding equation therefore simplifies to $\sigma_x^2 = \frac{1}{M}\int_{-\pi}^{\pi} S_{yy}(e^{j\omega})\frac{d\omega}{2\pi} = \frac{1}{M}\sigma_y^2$ ■

IV. FILTER AND QUANTIZER ASSUMPTIONS

Filter assumptions. The filters $F(e^{j\omega})$ of Fig. 1 and $F_k(e^{j\omega})$, $k = 0, 1, \ldots, L-1$, of Fig. 2 are assumed to be the synthesis filters of any L channels of an M-channel maximally decimated *orthonormal* filter bank. Although not necessary for developing the results of this paper, we will additionally choose the L channels of the M-channel maximally decimated *orthonormal* filter bank to be the most dominant ones in terms of subband energy. The model filters are therefore the so-called optimum energy compaction filters. This last constraint is motivated by the fairly recent result that this particular choice of filters minimize the mean square reconstruction error between the original signal $x(n)$ and its approximation $\hat{x}(n)$ [9], [10]. We would like however to emphasize that, unlike previous work, the filters in this paper are assumed to be of finite order. Working with ideal brick wall filters will obviously contradict the non-bandlimited assumption.

Quantizer assumption. As a convention for this paper, the box labeled $\mathcal{Q}$ represents a scalar uniform (PCM) quantizer and is modeled as an additive zero mean white noise source $q(n)$. Because the model filters are not ideal, the input $x(n)$ is a zero mean $(CWSS)_M$ process. Since the input to the quantizer $x(n)$ is a $(CWSS)_M$ process, its variance $\sigma_x^2(n)$ is a periodic function of n with period M. Define σ_x^2 to be the average variance of $x(n)$, i.e., $\sigma_x^2 = \frac{1}{M}\sum_{n=0}^{M-1}\sigma_x^2(n)$. Then, choose the fixed step size Δ in the uniform quantizer such that the quantization noise variance σ_q^2 is directly proportional to the average variance of the quantizer input $x(n)$, that is

$$\sigma_q^2 = c2^{-2b}\sigma_x^2 \tag{7}$$

where σ_q^2 is the quantization noise variance, c is a constant that depends on the statistical distribution of $x(n)$ and the overflow probability, and σ_x^2 is the average variance of the quantizer input. The above relation is justified for a PCM quantizer using 3 (or more) bits per sample (see chapter 4 in [11]). If the input to $\mathcal{Q}$ is wide-sense stationary, the above relation holds with σ_x^2 now denoting the actual variance of the WSS process.

V. INCREASING THE QUANTIZER RESOLUTION BY MULTIRATE FILTERING

Consider the set up shown in Fig. 5 for the single band model and in Fig. 14 for the multiband case. In the absence of the quantization, the two schemes are perfect reconstruction systems. In the presence of the quantizer, the output $\hat{x}(n)$ in Fig. 5 and Fig. 14 is equal to the original sequence $x(n)$ plus an error signal $e(n)$ due to

quantization. The following result shows that, by using the above schemes, a significant reduction in the average mean square error $\mathcal{E} \triangleq \frac{1}{M}\sum_{n=0}^{M-1} E\{e(n)\}^2$ can be obtained in comparison with the direct quantization of $x(n)$ shown in Fig. 12.

Theorem 5.1. *Consider the scheme of Fig. 14 where the L filters $F_k(e^{j\omega})$ are assumed to be any L channels of an M-channel critically sampled orthonormal filter bank. Under the above quantization noise assumption, the average mean square error (m.s.e) $\mathcal{E} \triangleq \frac{1}{M}\sum_{n=0}^{M-1} E\{\hat{x}(n) - x(n)\}^2$ is equal to $\frac{L}{M}\sigma_q^2$.*

Proof. Because the system is a perfect reconstruction one, the average error at the output is due only to the quantization noise. The quantization noise $q(n)$ is white and propagates through the L channels of Fig. 14. For the *kth* channel, the variance of $u_k(n)$ due to the noise passage through $F_k(e^{j\omega})$ is given by:

$$\sigma_{u_k}^2 = \sigma_q^2 \int_{-\pi}^{\pi} |F_k(e^{j\omega})|^2 \frac{d\omega}{2\pi} = \sigma_q^2 \tag{8}$$

The second equality follows because the filters have unit energy. The downsampling operation does not alter the variance of a signal. We therefore obtain $\sigma_{v_k}^2 = \sigma_{u_k}^2 = \sigma_q^2$ for all k. Using result 1 of section III, we can write

$$\mathcal{E} = \frac{1}{M}\sum_{k=0}^{L-1} \sigma_{v_k}^2 = \frac{L}{M}\sigma_q^2 \tag{9}$$

■

For the scheme of Fig. 5, the average m.s.e. $\mathcal{E}$ can be obtained directly by setting $L = 1$ and is therefore equal to $\frac{1}{M}\sigma_q^2$. The quantization noise variance σ_q^2 obtained by directly quantizing $x(n)$ as shown in Fig. 12 is now reduced by the oversampling factor M. The signal variance σ_x^2 on the other hand did not change. By expressing the interpolator M in the form 2^r, we can immediately see that we can get the same quantitative advantage of the oversampling PCM technique, namely, an increase in SNR by 3 db for every doubling of the oversampling factor. For example, for the single band case of Fig. 5, if $M = 2$, then, we get an SNR increase of 3 db whereas if $M = 4$, the SNR increment is by 6 db. Some important remarks are in order at this point :

1. In the oversampling PCM technique, the quantized bandlimited signal is typically downsampled after the low pass filter [6]. The SNR before and after the downsampler is the same and the increase in SNR is only due to a reduction in noise power. Similarly, the SNR before and after the interpolation filter in Fig. 5 does not change. However, the reason for the SNR increase before the interpolation filter is different from the one after the interpolation filter. In specific, at the input of the interpolation filter, the signal variance increases proportionally to M since $\sigma_y^2 = M\sigma_x^2$ and the noise power remains fixed. At the output of the interpolation filter, the signal variance doesn't change but the noise power decreases in proportion to M. In both cases, this amounts to the same SNR improvement. This last technical difference arises because our study assumes a statistical framework rather than a deterministic one (typical in A/D conversion applications) and because of our quantizer assumptions.

2. *Intuitive explanation of theorem* 5.1. The signal $x(n)$, modeled either as in Fig. 1 or Fig. 2, is oversampled and therefore, contains redundant information in the form of an excess of samples. It is by quantizing these extra

samples that we obtain the reduction in the quantization noise variance (equivalently in the mean square error). We are therefore effectively quantizing with a higher number of bits per sample. This trade off, between the quantization noise variance (effective quantizer resolution) and the sampling rate is the underlying principle of oversampled A/D converters.

3. *The role of the factor L in this analysis.* The parameter L, defined to be the number of channels in the multiband case, alternates between two extremes : $L = 1$ and $L = M$. When $L = 1$, we get the best SNR improvement at the expense of a more narrow class of inputs $x(n)$. When $L = M$, it is clear from (9) that no noise variance reduction is achieved since the class of signals is now unrestricted. We can also see this by noticing that the multirate interconnection in Fig. 14 becomes a perfect reconstruction filter bank that is signal independent. The parameter L therefore determines the tradeoff between the generality of the class of signals $x(n)$ and the reduction in quantization noise variance.

4. *A cascade of the scheme of Fig. 5 does not provide any further gain.* Using the scheme of Fig. 5, we obtained a reduction in noise by a factor M. If we use a cascade of the same filtering scheme as in Fig. 15, no further noise reduction is obtainable. Using the polyphase identity [5] and keeping in mind that $|F(e^{j\omega})|^2$ is Nyquist(M), the product filter $F(e^{j\omega})\tilde{F}(e^{j\omega})$ together with the expander and decimator reduces to an identity system. Fig. 15 therefore simplifies to Fig. 5 and the average m.s.e is the same.

VI. QUANTIZING AT LOWER RATE

A consequence of the previous results and discussion is then the natural question: what if the discrete time filtering of the oversampled signal is not a major burden ? If we know that $x(n)$ can be modeled quite accurately by the filter $F(e^{j\omega})$ of Fig. 1 or the filters $F_k(e^{j\omega})$, $k = 0, 1, \ldots, L-1$, of Fig. 2, we filter and downsample $x(n)$ accordingly to obtain either $y(n)$ or $y_k(n)$, $k = 0, 1, \ldots, L-1$. The quantization systems for the two models are shown in Fig. 7 and Fig. 16 respectively. We can then in principle quantize the decimated signal $y(n)$ in Fig. 7 with $\hat{b} = Mb$ bits per sample or the signals $y_k(n)$, $k = 0, 1, \ldots, L-1$, of Fig. 16 with an average number of bits per sample $\hat{b} = \frac{M}{L}b$ bits. This situation is equivalent to fixing the bit rate (number of bits per second) to be equal to b in order to trade quantization resolution with sampling rate. Moreover, for the multiband case, we can allocate bits b_k to the driving signals $y_k(n)$ in an "appropriate" manner. At this point, we will however assume that the goal is to actually obtain a reduction in the bit rate. To achieve this, we let $\hat{b}$ be equal to b for both cases and analyze the quantization systems of Fig. 7 and Fig. 16 under this condition. By fixing the number of bits per sample and decreasing the signal rate, the bit rate will automatically decrease by M/L. However, since the quantizer resolution did not increase, the quantization noise variance should not differ from the direct quantization case of Fig. 12. This last statement is verified formally in the next theorems.

Theorem 6.1. *Consider the scheme of Fig. 7. Using a fixed number of bits per sample b to quantize $y(n)$, the average mean square error $\mathcal{E}$ is equal to σ_q^2, where σ_q^2 is the noise variance obtained from directly quantizing $x(n)$ using b bits per sample.*

Proof. Let σ_q^2 be the noise variance of Fig. 12 and $\mathcal{E}$ be the average mean square error of Fig. 7. Using (7), we can write $\sigma_q^2 = c2^{-2b}\sigma_x^2$. But, by result 2 of section III, $\mathcal{E} = \frac{1}{M}c2^{-2b}\sigma_y^2 = \frac{1}{M}c2^{-2b}M\sigma_x^2 = \sigma_q^2$, where σ_x^2 is the average variance of $x(n)$. ■

The theorem indicates that, for the single band model and under a fixed number of quantizer bits b, quantizing the lower rate signal $y(n)$ is as accurate as directly quantizing $x(n)$. This is expected and is in fact consistent with the observation of section V regarding the tradeoff between the average m.s.e due to quantization and the rate of the signal. The next theorem for the multiband case gives a similar conclusion.

Theorem 6.2. *Consider the scheme of Fig. 16. Assume that we quantize $y_k(n)$ at b bits per sample for all k. Then, the average mean square error $\mathcal{E}$ is equal to σ_q^2, where σ_q^2 is the noise variance obtained from directly quantizing $x(n)$ using b bits per sample.*

Proof. The average mean square error at the output of Fig. 16 is equal to

$$\mathcal{E} = \frac{1}{M}\sum_{k=0}^{L-1}\sigma_{q_k}^2 = \frac{1}{M}c2^{-2b}\sum_{k=0}^{L-1}\sigma_{y_k}^2 \tag{10}$$

where b denotes the *fixed* number of bits allocated to the kth channel quantizer. The noise variance σ_q^2 in Fig. 12 is equal to $c2^{-2b}\sigma_x^2$, which in turn is equal to (10). ■

VII. NOISE SHAPING BY TIME-INVARIANT PRE- AND POST FILTERS

Following the philosophy of sigma-delta modulators, we now perform noise shaping to achieve a further reduction in the average mean square error. To accomplish this, we propose using LTI pre- and post filters around the PCM quantizer as shown in Fig. 6 for the single band model and in Fig. 17 for the multiband model. We first use a prefilter $P(e^{j\omega})$ and assume that the postfilter is its inverse. We then relax this condition and assume a more general postfilter $V(e^{j\omega})$. The goal is to optimize these filters such that the average m.s.e at the output of either quantization system is minimized. The noise shaping filters to be optimized are not constrained to be rational functions (i.e., of finite order) and non causal solutions, for example, are accepted.

Although our quantizer design assumptions are the same as before, the quantizer input is not anymore the $(CWSS)_M$ process $x(n)$, but a filtered version of it, which we denote by $z(n)$. Following (7), the noise variance in this case is given by $\sigma_q^2 = c2^{-2b}\sigma_z^2$ where σ_z^2 is the average variance of the process $z(n)$. We emphasize that $z(n)$ is a $(CWSS)_M$ process since the output of a linear time invariant filter driven by a $(CWSS)_M$ process is also $(CWSS)_M$ [8]. It is then possible to express σ_z^2 in terms of the prefilter $P(e^{j\omega})$ and the so called average power spectral density (see below) of the process $x(n)$, denoted by $\hat{S}_{xx}(e^{j\omega})$, as follows :

$$\sigma_z^2 = \frac{1}{M}\int_{-\pi}^{\pi}|P(e^{j\omega})|^2\hat{S}_{xx}(e^{j\omega})\frac{d\omega}{2\pi} \tag{11}$$

The proof of (11) can be found in appendix C. The average power spectral density is a familiar concept that arises when "stationarizing" a $(CWSS)_M$ process [12],[13],[14] and satisfies the well known properties of the

power spectrum of a WSS process. It is defined to be the discrete time fourier transform of the time averaged autocorrelation function $\hat{R}_{xx}(k)$ given by $\frac{1}{M}\sum_{n=0}^{M-1} E[x(n)x^*(n-k)]$. Another interpretation of the average power spectral density which can be physically more appealing is based on the concept of phase randomization and is reviewed in appendix B. Finally, if $x(n)$ is modeled as in Fig. 1, it can be shown that :

$$\hat{S}_{xx}(e^{j\omega}) = \frac{1}{M} S_{yy}(e^{j\omega M})|F(e^{j\omega})|^2 \tag{12}$$

whereas if the signal satisfies the multiband model of Fig. 2, the average power spectral density takes the following form :

$$\hat{S}_{xx}(e^{j\omega}) = \frac{1}{M}\mathbf{F}^{\dagger}(e^{j\omega})\mathbf{S_y}(e^{j\omega M})\mathbf{F}(e^{j\omega}) \tag{13}$$

where $\mathbf{F}(e^{j\omega}) = (\, F_0(e^{j\omega}) \quad F_1(e^{j\omega}) \quad \ldots \quad F_{L-1}(e^{j\omega})\,)^T$ and $\mathbf{S_y}(e^{j\omega})$ is the $L \times L$ power spectral density matrix of the L WSS inputs $y_k(n)$. Note that, when the signals $y_k(n)$ are uncorrelated, equation (13) simplifies to $\frac{1}{M}\sum_{k=0}^{L-1} S_{y_k}(e^{j\omega M})|F_k(e^{j\omega})|^2$. The proofs of (12) and (13) are given in appendix D. The expression (12) was derived previously in [8] for the special case where $F(e^{j\omega})$ is an anti-alias(M) filter. Furthermore, the authors prove that the output process $x(n)$ is WSS if and only if $F(e^{j\omega})$ is an anti-alias(M) filter. In summary, the statistical properties of the output $x(n)$ of Fig. 1 depend on $F(e^{j\omega})$. If the filter is an anti-alias(M) filter, then, $x(n)$ is WSS with a power spectral density $S_{xx}(e^{j\omega})$ in the same form as (12). Otherwise, $x(n)$ is a $(CWSS)_M$ process and in this case, the average power spectral density $\hat{S}_{xx}(e^{j\omega})$ is given by (12).

7.1. Case where the postfilter is the inverse of the prefilter

Theorem 7.1.1. *Consider the scheme of Fig. 17 under the same assumptions of section IV. The optimum prefilter $P(e^{j\omega})$ that minimizes the average mean square reconstruction error has the following magnitude squared response:*

$$|P_{opt}(e^{j\omega})|^2 = \frac{\sqrt{(\sum_{i=0}^{L-1}|F_i(e^{j\omega})|^2)}}{\sqrt{\hat{S}_{xx}(e^{j\omega})}} \tag{14}$$

Proof. We first observe that in the absence of quantization, the system of Fig. 17 is a perfect reconstruction system. Therefore, the average mean square reconstruction error $\sigma_e^2 = \frac{1}{M}\sum_{n=0}^{M-1} E[\hat{x}(n) - x(n)]^2$ at the output is due only to the noise signal. Let $v_k(n)$ be the filtered noise component in the kth channel of the L-channel filter bank of Fig. 17. The variance of this signal $\sigma_{v_k}^2$ is equal to

$$\sigma_{v_k}^2 = \int_{-\pi}^{\pi} \sigma_q^2 \frac{|F_k(e^{j\omega})|^2}{|P(e^{j\omega})|^2}\frac{d\omega}{2\pi} \tag{15}$$

Since the downsampling operation does not change the variance of a process, we can write

$$\sigma_e^2 = \frac{1}{M}\sum_{k=0}^{L-1}\sigma_{v_k}^2 = \sigma_q^2\frac{1}{M}\int_{-\pi}^{\pi}\frac{\sum_{k=0}^{L-1}|F_k(e^{j\omega})|^2}{|P(e^{j\omega})|^2}\frac{d\omega}{2\pi} \tag{16}$$

Using (7) and (11), we get

$$\sigma_e^2 = \frac{c2^{-2b}}{M}\int_{-\pi}^{\pi}\hat{S}_{xx}(e^{j\omega})|P(e^{j\omega})|^2\frac{d\omega}{2\pi}\int_{-\pi}^{\pi}\frac{\sum_{k=0}^{L-1}|F_k(e^{j\omega})|^2}{|P(e^{j\omega})|^2}\frac{d\omega}{2\pi} \tag{17}$$

To find the optimum prefilter $P(e^{j\omega})$, we apply Cauchy-Schwartz inequality to (17) to obtain:

$$\sigma_e^2 \geq \frac{c2^{-2b}}{M}\left(\int_{-\pi}^{\pi}\sqrt{\hat{S}_{xx}(e^{j\omega})\left(\sum_{i=0}^{L-1}|F_i(e^{j\omega})|^2\right)}\frac{d\omega}{2\pi}\right)^2 \tag{18}$$

Since this lower bound is independent of $P(e^{j\omega})$, it is indeed the required minimum and is achieved iff

$$\sqrt{\hat{S}_{xx}(e^{j\omega})}|P(e^{j\omega})| = \frac{\sqrt{\left(\sum_{i=0}^{L-1}|F_i(e^{j\omega})|^2\right)}}{|P(e^{j\omega})|} \tag{19}$$

which gives (14). ■

A number of observations should be made at this point. First, the optimum filter is not unique since the phase response is not specified. Second, the above derivation assumes that the input average spectrum $\hat{S}_{xx}(e^{j\omega}) \neq 0$ for all ω. The assumption is a reasonable one because $x(n)$ is assumed to be non bandlimited and therefore $\hat{S}_{xx}(e^{j\omega})$ cannot be identically zero on a segment of $[0, 2\pi)$. If $\hat{S}_{xx}(e^{j\omega})$ has an isolated zero for some ω, then, the resulting prefilter will have a zero on the unit circle and is therefore unstable. In any case, a practical system would use only a stable rational approximation of the ideal solution. Finally, we note that the optimum filter for the scheme of Fig. 6 can be obtained again as a special case by setting $L = 1$ in (14). The optimum prefilter will then have the following magnitude squared response:

$$|P_{opt}(e^{j\omega})|^2 = \frac{|F(e^{j\omega})|}{\sqrt{\hat{S}_{xx}(e^{j\omega})}} \tag{20}$$

and can be regarded as a multirate extension of the half whitening filter [11]. Using (20), we can derive an interesting expression for the coding gain of the scheme of Fig. 6.

Theorem 7.1.2. *With the optimum choice of the pre- and post filter, the coding gain expression for the scheme of Fig. 6 is*

$$\mathcal{G}_{opt} = \frac{M\int_{-\pi}^{\pi} S_{yy}(e^{j\omega})\frac{d\omega}{2\pi}}{\left(\int_{-\pi}^{\pi}\sqrt{S_{yy}(e^{j\omega})}\frac{d\omega}{2\pi}\right)^2} = M \cdot \mathcal{G}_{hw} \tag{21}$$

where $\mathcal{G}_{hw}$ is the half whitening coding gain of the WSS process $y(n)$ [11].

Proof. By definition, the coding gain of the system is given by

$$\mathcal{G}_{opt} = \frac{\sigma_q^2}{\mathcal{E}_{opt}} = \frac{\sigma_x^2}{\left(\frac{1}{M}\int_{-\pi}^{\pi}\sqrt{\hat{S}_{xx}(e^{j\omega})}|F(e^{j\omega})|\frac{d\omega}{2\pi}\right)^2} = \frac{M\int_{-\pi}^{\pi}\hat{S}_{xx}(e^{j\omega})\frac{d\omega}{2\pi}}{\left(\int_{-\pi}^{\pi}\sqrt{\hat{S}_{xx}(e^{j\omega})}|F(e^{j\omega})|\frac{d\omega}{2\pi}\right)^2} \tag{22}$$

Substituting (12) in (22) and simplifying, we get

$$\mathcal{G}_{opt} = \frac{M\int_{-\pi}^{\pi} S_{yy}(e^{jM\omega})|F(e^{j\omega})|^2\frac{d\omega}{2\pi}}{\left(\int_{-\pi}^{\pi}\sqrt{S_{yy}(e^{jM\omega})}|F(e^{j\omega})|^2\frac{d\omega}{2\pi}\right)^2} \tag{23}$$

The integrals in both the numerator and the denominator can be interpreted as the variance of a WSS random process with a power spectrum density equal to $S_{yy}(e^{jM\omega})|F(e^{j\omega})|^2$ and $\sqrt{S_{yy}(e^{jM\omega})}|F(e^{j\omega})|^2$ respectively. But

we know that downsampling a WSS process produces another WSS process with the same variance. Therefore, we can write

$$\mathcal{G}_{opt} = \frac{M\int_{-\pi}^{\pi}(S_{yy}(e^{jM\omega})|F(e^{j\omega})|^2)\downarrow_M \frac{d\omega}{2\pi}}{(\int_{-\pi}^{\pi}(\sqrt{S_{yy}(e^{jM\omega})}|F(e^{j\omega})|^2)\downarrow_M \frac{d\omega}{2\pi})^2} \tag{24}$$

Using the fact that $(S_{yy}(e^{jM\omega})|F(e^{j\omega})|^2)\downarrow_M = S_{yy}(e^{j\omega})(|F(e^{j\omega})|^2)\downarrow_M$ and that $(|F(e^{j\omega})|^2)\downarrow_M = 1$, we get (21). ■

The factor M in (21) is again due to the oversampled nature of the signal $x(n)$. It is interesting to note that the noise shaping contribution to $\mathcal{G}_{opt}$ in (21), which we denote by $\mathcal{G}_{hw}$, is exactly the *coding gain we would obtain by half whitening the WSS process $y(n)$ in the usual way* [11]. By appealing to the Cauchy Schwartz inequality again, we can show that $\mathcal{G}_{hw} \geq 1$ with equality iff the power spectral density $S_{yy}(e^{j\omega})$ is a constant, i.e., $y(n)$ is white noise. Therefore, for the particular system of Fig. 6, we will not get additional coding gain by noise shaping if the driving WSS process $y(n)$ in Fig. 1 is white noise. For completeness, we would like to mention that the following expression for the coding gain of Fig. 17 (the multiband case) can be derived under the assumption that the JWSS processes $y_k(n)$, $k = 0, 1, \ldots, L-1$, are uncorrelated :

$$\mathcal{G}_{opt} = \frac{M\int_{-\pi}^{\pi}\sum_{k=0}^{L-1} S_{y_k}(e^{jM\omega})|F_k(e^{j\omega})|^2 \frac{d\omega}{2\pi}}{(\int_{-\pi}^{\pi}\sqrt{\sum_{i=0}^{L-1} S_{y_i}(e^{jM\omega})|F_i(e^{j\omega})|^2}\sqrt{\sum_{n=0}^{L-1}|F_n(e^{j\omega})|^2}\frac{d\omega}{2\pi})^2} \tag{25}$$

7.2. Using a more general postfilter

Consider now the more general system of Fig. 8 where the postfilter is not assumed to be the inverse of the prefilter. The multiband case is shown in Fig. 18. The goal is to jointly optimize the prefilter $P(e^{j\omega})$ and the postfilter $V(e^{j\omega})$ to again minimize the average m.s.e $\stackrel{\Delta}{=} 1/M\sum_{n=0}^{M-1} E\{\hat{x}(n) - x(n)\}^2$ under the following assumptions:

1. The input $x(n)$ is assumed to be a zero mean real wide sense stationary process.
2. The input $x(n)$ and the quantization noise $q(n)$ are uncorrelated processes, i.e., $E\{x(n)q(m)\} = 0 \; \forall \, n, m$.
3. The quantization noise $q(n)$ is white with variance σ_q^2 as in (7).
4. The filters $P(e^{j\omega})$ and $V(e^{j\omega})$ are not constrained to be rational functions and can be non causal.
5. The power spectral density $S_{xx}(e^{j\omega})$ is positive for all ω. Furthermore, for the derivation of the optimum prefilter, we will also require $S_{xx}(e^{j\omega})$ and its first derivative to be continuous functions of frequency.

To solve the above problem, our approach will be the following : First, consider the single band case of Fig. 8. Unlike previous quantization schemes, we observe that in the absence of the quantizer, the scheme of Fig. 8 is *not* a perfect reconstruction system. The error sequence $e(n) = \hat{x}(n) - x(n)$ has in fact two components: one due to the mismatch between the pre- and post filters and the other due to the filtered quantization noise. We cannot therefore simply minimize the mean square reconstruction error before the downsampler as in the previous sections. Using the m.s.e definition given above, we derive an expression for the average mean square reconstruction error $1/M\sum_{n=0}^{M-1} E\{e^2(n)\}$ in terms of the filters and the average power spectrum of the signal $x(n)$ and noise $q(n)$. The use of the average power spectral density of the $(CWSS)_M$ input $x(n)$ in this case is not theoretically correct, even under the same quantizer assumptions as before. Nevertheless, it is necessary to work with this quantity to

obtain any meaningful comparison between this more general set up and the one of the previous subsection. The calculus of variation is used as a tool to derive closed form expressions for both the optimum pre- and post filters which are then used to obtain the coding gain expression of Fig. 8. Finally, we will show how to the generalize the results for the multiband case of Fig. 18.

Theorem 7.2.1. *For a fixed prefilter $P(e^{j\omega})$ and a given filter $F(e^{j\omega})$, the optimum postfilter $V_{opt}(e^{j\omega})$ is:*

$$V_{opt}(e^{j\omega}) = \frac{1}{P(e^{j\omega})} \frac{\hat{S}_{xx}(e^{j\omega})}{\hat{S}_{xx}(e^{j\omega}) + \frac{c2^{-2b}}{|P(e^{j\omega})|^2}\int_{-\pi}^{\pi} \hat{S}_{xx}(e^{j\omega})|P(e^{j\omega})|^2 \frac{d\omega}{2\pi}} \tag{26}$$

Proof. The average mean square reconstruction error can be expressed as follows:

$$\begin{aligned}
\mathcal{E} &= \frac{1}{M}\sum_{n=0}^{M-1} E\{e^2(n)\} \\
&= E\{x^2(n)\} + \frac{1}{M}\sum_{n=0}^{M-1} E\{\hat{x}^2(n)\} - \frac{1}{M}\sum_{n=0}^{M-1} E\{\hat{x}(n)x(n)\} - \frac{1}{M}\sum_{n=0}^{M-1} E\{x(n)\hat{x}(n)\} \\
&= \int_{-\pi}^{\pi} \hat{S}_{xx}(e^{j\omega})\frac{d\omega}{2\pi} + \frac{1}{M}\int_{-\pi}^{\pi} \hat{S}_{xx}(e^{j\omega})|P(e^{j\omega})|^2|V(e^{j\omega})|^2|F(e^{j\omega})|^2\frac{d\omega}{2\pi} \\
&+ \frac{1}{M}\int_{-\pi}^{\pi} \sigma_q^2|V(e^{j\omega})|^2|F(e^{j\omega})|^2\frac{d\omega}{2\pi} - \frac{1}{M}2\int_{-\pi}^{\pi} \hat{S}_{xx}(e^{j\omega})|F(e^{j\omega})|^2\Re\{P(e^{j\omega})V(e^{j\omega})\}\frac{d\omega}{2\pi}
\end{aligned} \tag{27}$$

where $\Re$ stands for the real part. First, observe that the average m.s.e dependency on the phase of the filters appears only in the last term. To minimize (27) with respect to the phase of the filters, the product $P(e^{j\omega})V(e^{j\omega})$ must be zero phase. To see this, simply set $P(e^{j\omega}) = |P(e^{j\omega})|e^{j\phi(\omega)}$ and $V(e^{j\omega}) = |V(e^{j\omega})|e^{j\Phi(\omega)}$. The real part of $P(e^{j\omega})V(e^{j\omega})$ is equal to $|V(e^{j\omega})||P(e^{j\omega})|\cos(\phi(\omega)+\Phi(\omega))$. To minimize (27), $\cos(\phi(\omega)+\Phi(\omega))$ must be equal to one. Dropping the real notation $\Re$ in (27), we now turn to the magnitude squared response of the filters. We first fix the prefilter $P(e^{j\omega})$ and optimize $|V(e^{j\omega})|$. This can be done by applying the Euler-Lagrange equation from the calculus of variation theory [15] to (27). The resulting expression is (26). ∎

It is interesting to note that the post filter is independent of $F(e^{j\omega})$. Substituting (26) into (27), we obtain the following average m.s.e expression :

$$\mathcal{E}(|P|^2, b) = \int_{-\pi}^{\pi} \frac{\hat{S}_{xx}(e^{j\omega})(\hat{S}_{xx}(e^{j\omega})|P(e^{j\omega})|^2(M-|F(e^{jw})|^2) + c2^{-2b}M\int_{-\pi}^{\pi}\hat{S}_{xx}(e^{ju})|P(e^{ju})|^2\frac{du}{2\pi})}{\hat{S}_{xx}(e^{j\omega})|P(e^{jw})|^2 + c2^{-2b}\int_{-\pi}^{\pi}\hat{S}_{xx}(e^{ju})|P(e^{ju})|^2\frac{du}{2\pi}}\frac{d\omega}{2\pi} \tag{28}$$

The above equation is only a function of the magnitude squared response of the prefilter. From this point on, the problem under study is very similar to the one analyzed recently in [16] and in fact, becomes exactly the same by setting M and $F(e^{j\omega})$ to unity in equation (28). We will therefore omit the proofs of the upcoming theorems referring the reader to [16].

Theorem 7.2.2. *The squared magnitude response $|P_{opt}(e^{jw})|^2$ that minimizes $\mathcal{E}(|P|^2, b)$, given in (28), is also the solution of the following constrained optimization problem:*

$$\min_{|P(e^{jw})|^2} \quad \int_{-\pi}^{\pi} \frac{\hat{S}_{xx}(e^{j\omega})(\hat{S}_{xx}(e^{j\omega})|P(e^{j\omega})|^2(1-|F(e^{jw})|^2) + c2^{-2b})}{\hat{S}_{xx}(e^{j\omega})|P(e^{jw})|^2 + c2^{-2b}}\frac{d\omega}{2\pi} \tag{29}$$

subject to:

$$\int_{-\pi}^{\pi} \hat{S}_{xx}(e^{j\omega})|P(e^{j\omega})|^2\frac{d\omega}{2\pi} = 1 \tag{30}$$

Theorem 7.2.3. *The prefilter* $|P_{opt}(e^{j\omega})|^2$ *that minimizes (29) under the constraint (30) must have a magnitude response* $|P_{opt}(e^{j\omega})|^2$ *in the following form:*

$$|P_{opt}(e^{j\omega})|^2 = \max\left(0, \frac{|F(e^{j\omega})|}{\sqrt{\hat{S}_{xx}(e^{j\omega})}}\left(\frac{1+c2^{-2b}}{\int_{-\pi}^{\pi}\sqrt{\hat{S}_{xx}(e^{j\omega})}|F(e^{j\omega})|\frac{d\omega}{2\pi}} - \frac{c2^{-2b}}{\sqrt{\hat{S}_{xx}(e^{j\omega})}}\right)\right) \forall \quad \omega \in [-\pi,\pi] \tag{31}$$

Theorem 7.2.4. *With the optimal choice of pre- and postfilters, the coding gain expression for the scheme of Fig. 8 is*

$$\mathcal{G}_{opt} = (1+c2^{-2b})M\mathcal{G}_{hw} \tag{32}$$

as long as $|P_{opt}(e^{j\omega})|^2$ *in (31) is never set to zero* $\forall\ \omega$. *Here,* $\mathcal{G}_{hw}$ *is again the half whitening coding gain of the WSS process* $y(n)$.

Note that in this case the coding gain of the more general set up is a concatenation of three factors : $\mathcal{G}_{hw}$ due to the noise shaping, the oversampling factor M due to the signal model and $1+c2^{-2b}$ due to using a more general form of pre- and post filters.

To conclude this section, we would like to repeat the same procedure for the more general scheme of Fig. 18. We claim that, for this case, the optimum postfilter is still given by (26) and the optimum pre- filter magnitude squared response expression is obtained from (31) by simply replacing $|F(e^{j\omega})|$ by $\sqrt{\sum_{k=0}^{L-1}|F_k(e^{j\omega})|^2}$. To prove this, the key is to derive an expression for the average mean square reconstruction error of Fig. 18. Clearly, if we can show that $\mathcal{E}$ for the multiband case can be expressed as

$$\begin{aligned}\mathcal{E} &= E\{x^2(n)\} + \frac{1}{M}\sum_{n=0}^{M-1}E\{\hat{x}^2(n)\} - \frac{1}{M}\sum_{n=0}^{M-1}E\{\hat{x}(n)x(n)\} - \frac{1}{M}\sum_{n=0}^{M-1}E\{x(n)\hat{x}(n)\} \\ &= \int_{-\pi}^{\pi}\hat{S}_{xx}(e^{j\omega})\frac{d\omega}{2\pi} + \frac{1}{M}\int_{-\pi}^{\pi}\hat{S}_{xx}(e^{j\omega})|P(e^{j\omega})|^2|V(e^{j\omega})|^2\sum_{k=0}^{L-1}|F_k(e^{j\omega})|^2\frac{d\omega}{2\pi} \\ &+ \frac{1}{M}\int_{-\pi}^{\pi}\sigma_q^2|V(e^{j\omega})|^2\sum_{k=0}^{L-1}|F(e^{j\omega})|^2\frac{d\omega}{2\pi} - \frac{1}{M}2\Re\int_{-\pi}^{\pi}\hat{S}_{xx}(e^{j\omega})P(e^{j\omega})V(e^{j\omega})\sum_{k=0}^{L-1}|F(e^{j\omega})|^2\frac{d\omega}{2\pi}\end{aligned} \tag{33}$$

then, from the previous analysis, the above claim follows immediately. To derive (33), we need to only consider the second term and one of the cross terms. The second term $1/M\sum_{n=0}^{M-1}E\{\hat{x}^2(n)\}$ is the variance of the signal estimate at the output of Fig. 18. But from result 2 of section III, we know that it is equal to $1/M\sum_{k=0}^{L-1}\sigma_{y_k}^2$ where $\sigma_{y_k}^2$ is the variance of the signal estimate before the kth channel downsampler, $k=0,\ldots,L-1$. Substituting with $\sigma_{y_k}^2$ in this last relation, we obtain the second and third integral in (33). Consider now one of the cross terms, say $1/M\sum_{n=0}^{M-1}E\{\hat{x}(n)x(n)\}$. We can rewrite $\hat{x}(n)$ as $\sum_{k=0}^{L-1}\hat{x}_k(n)$ where $\hat{x}_k(n)$ is the signal estimate at the output of the kth channel. By the linearity of the expectation, this gives $1/M\sum_{k=0}^{L-1}\sum_{n=0}^{M-1}E\{\hat{x}_k(n)x(n)\}$. By interpreting the single band case as the kth channel, the last integral follows easily. Equation (33) is therefore established and the claim is proved.

Example 7.1. *Case of a MA(1) process* $y(n)$. Assume that the input $x(n)$ is modeled as in Fig. 1 with $M=2$ and $F(e^{j\omega}) = \frac{1}{\sqrt{2}}(1+z^{-1})$. Let the driving WSS signal $y(n)$ be a zero mean gaussian MA(1) process with an

autocorrelation sequence in the form

$$R_{yy}(k) = \begin{cases} 1 & k = 0. \\ \frac{\theta}{1+\theta^2} & k = 1, -1. \\ 0 & \text{otherwise.} \end{cases}$$

The MA(1) process has to have $\frac{|R_{yy}(1)|}{R_{yy}(0)} \leq 1/2$ to ensure that the power spectral density is indeed non negative. We therefore restrict θ to be between -1 and 1. The power spectrum of the MA(1) process is given by:

$$S_{yy}(e^{j\omega}) = 1 - 2\frac{\theta}{(1+\theta^2)}cos(\omega) \tag{34}$$

Substituting (34) in (21), the coding gain expression of the scheme Fig. 6 becomes

$$\mathcal{G}_{opt} = \frac{2(1+\theta^2)}{\left(\int_{-\pi}^{\pi} \sqrt{(1+\theta^2-2\theta cos(\omega))}\, \frac{d\omega}{2\pi}\right)^2} \tag{35}$$

The integral in (35) is equal to $F(-0.5\ , -0.5\ ;\ 1\ ;\ \theta^2)$ where $F(a\ ,\ b\ ;\ c\ ;\ d)$ is Gauss's hypergeometric function. From [17], $F(-0.5\ ,\ -0.5\ ;\ 1\ ;\theta^2)$ can be rewritten as $(1\ +\ \theta)F(-0.5\ ,\ 0.5\ ;\ 1\ ;4\theta/(1\ +\ \theta)^2)$. This, in turn, can be simplified to $(1\ +\ \theta)\frac{2}{\pi}E(2\sqrt{(|\theta|)}/(1\ +\ \theta))$ where $E(.)$ is the complete elliptic integral of the second kind. The coding gain of the more general system can be obtained by multiplying (35) by $(1+c2^{-2b})$ and obviously depends on the number of bits b. The plots of the coding gain are illustrated in Fig. 19 for $b = 3$ and $c = 2.4$.

Example 7.2. *Case of an AR(1) process $y(n)$.* With the same assumptions as in example 7.1, let the driving signal $y(n)$ be a zero mean gaussian AR(1) process with an autocorrelation sequence in the form $R_{yy}(k) = \rho^{|k|}$ where ρ is between 0 and 1. The power spectrum of the AR(1) process is

$$S_{yy}(e^{j\omega}) = \frac{1-\rho^2}{1+\rho^2-2\rho cos(\omega)} \tag{36}$$

Substituting (36) in (21), the coding gain expression for the scheme of Fig. 6 is as follows:

$$\mathcal{G}_{opt} = \frac{2}{(1-\rho^2)\left(\int_{-\pi}^{\pi} \frac{1}{\sqrt{(1+\rho^2-2\rho cos(\omega))}}\, \frac{d\omega}{2\pi}\right)^2} \tag{37}$$

The integral in (37) is equal to $\frac{2}{\pi}K(\rho)$ where $K(\rho)$ is the complete elliptic integral of the first kind [17]. Again, the coding gain of the more general system is obtained by multiplying (37) by $(1+c2^{-2b})$. The plots of the coding gain are shown in Fig. 20 for $b = 3$ and $c = 2.4$.

VIII. NOISE SHAPING BY $(LPTV)_M$ PRE- AND POST FILTERS

In this section, we consider using $(LPTV)_M$ pre- and post filters instead of LTI ones surrounding a periodically time varying $((PTV)_M)$ quantizer. Since the signal model $x(n)$ is $(CWSS)_M$, restricting ourselves to linear time invariant noise shaping filters and quantizers is a loss of generality. Any optimum configuration for such processes should consist of $(LPTV)_M$ filters surrounding a $((PTV)_M)$ quantizer. Using some well known multirate results,

it can be shown that this new quantization configuration is equivalent to an M-channel maximally decimated filter bank with M subband quantizers [5]. We will further impose the perfect reconstruction condition in the absence of quantization by confining ourselves to the class of perfect reconstruction filter banks. It follows that $\mathbf{R}(e^{j\omega}) = \mathbf{E}^{-1}(e^{j\omega})$ where $\mathbf{E}(e^{j\omega})$ and $\mathbf{R}(e^{j\omega})$ denote respectively the analysis and synthesis polyphase matrices [17]. Equivalently, the analysis and synthesis filters satisfy the biorthogonality condition: $(P_k(e^{j\omega})Q_m(e^{j\omega}))|\downarrow_M = \delta(m-k)$ for all k, m. The goal is then to find the set of M analysis and synthesis filters, $P_k(e^{j\omega})$ and $Q_k(e^{j\omega})$ (equivalently the analysis and synthesis polyphase matrices), that minimize the average mean square error at the output due to the quantization noise. Because the general $(LPTV)_M$ problem is difficult to track analytically, we will only study two special forms of the above set up. The first case assumes that $\mathbf{E}(e^{j\omega})$ is diagonal with diagonal elements equal to $V_k(e^{j\omega})$. It follows that $\mathbf{R}(e^{j\omega})$ is also diagonal with diagonal elements equal to $\frac{1}{V_k(e^{j\omega})}$ for each k. The second case assumes that $\mathbf{E}(e^{j\omega})$ is paraunitary and we choose $\mathbf{R}(e^{j\omega}) = \mathbf{E}^{\dagger}(e^{j\omega})$. Alternatively, the synthesis filters $Q_k(e^{j\omega})$ are equal to $\tilde{P}_k(e^{j\omega})$ for each k and $(P_k(e^{j\omega})\tilde{P}_m(e^{j\omega}))|\downarrow_M = \delta(m-k)$ for all k, m. These two special forms are intermediate between one extreme (the LTI case) and the other (the general $(LPTV)_M$ case).

8.1. Letting the synthesis filter be the inverse of the analysis filter

Let $\mathbf{E}(e^{j\omega})$ be a diagonal matrix with diagonal elements equal to $V_k(e^{j\omega})$ and $\mathbf{R}(e^{j\omega})$ be also diagonal with diagonal elements equal to $\frac{1}{V_k(e^{j\omega})}$ for each k. The quantization configuration is shown in Fig. 9 for the single band case and Fig. 21 for the multiband case. The scalar quantizers labeled $\mathcal{Q}$ are modeled as additive noise sources $q_k(n)$ and individually satisfy relation (7). Throughout this section, we will assume that the subband quantization noise sources $q_k(n)$ are white and pairwise uncorrelated, i.e., the noise power spectral density matrix is given by

$$\mathbf{S}_{qq}(e^{j\omega}) = \begin{pmatrix} \sigma_{q_0}^2 & 0 & \dots & 0 \\ 0 & \sigma_{q_1}^2 & \dots & 0 \\ \vdots & \vdots & \ddots & \vdots \\ 0 & \dots & \dots & \sigma_{q_{M-1}}^2 \end{pmatrix} \tag{38}$$

The goal is then to jointly allocate the subband bits b_k under a fixed bit rate

$$b = \frac{1}{M}\sum_{k=0}^{M-1} b_k \tag{39}$$

and optimize $V_k(e^{j\omega})$ in order to minimize the average m.s.e at the output of Fig. 9 and Fig. 21. Our strategy is as follows: we first find the optimum solution for the single band case of Fig. 9. Then, by interpreting the single band model as one of the L channels of the more general multiband case, the optimum solution for Fig. 21 follows.

Theorem 8.1.1. *Consider the scheme of Fig. 9 under the above assumptions. The optimum filter $V_{opt}(e^{j\omega})$ that minimizes the average mean square reconstruction error at the output is* **independent of** *k and has the following magnitude squared response:*

$$|V_{opt}(e^{j\omega})|^2 = \frac{1}{\sqrt{S_{yy}(e^{j\omega})}} \tag{40}$$

where $S_{yy}(e^{j\omega})$ is the power spectrum of the WSS process $y(n)$ in Fig. 1. With the above optimum filter expression, the coding gain of Fig. 9 is then given by :

$$\mathcal{G}_{opt} = \frac{\sigma_y^2}{M(\prod_{k=0}^{M-1} \int_{-\pi}^{\pi} \sqrt{S_{yy}(e^{j\omega})}|\tilde{R}_k(e^{j\omega})|^2 \frac{d\omega}{2\pi})^{2/M}} \tag{41}$$

where $\tilde{R}_k(e^{j\omega})$ is the kth polyphase component of $\tilde{F}(e^{j\omega})$.

Proof. Since the system has the perfect reconstruction property in the absence of quantization, the error $e(n)$ at the output is simply the filtered quantization noise signal. After the downsampler, the filtered noise component $w(n)$ is WSS. By result 2 of section III, $\mathcal{E} = \frac{1}{M}\sigma_w^2$. To compute σ_w^2, we express the filter $\tilde{F}(e^{j\omega})$ in terms of its M polyphase components $\tilde{R}_k(e^{j\omega})$. Because the input signal $x(n)$ is modeled as in Fig. 1, we can also invoke the polyphase identity (see [5] pp. 133) at the input to simplify Fig. 9 to Fig. 22 (The interpolation filter was not drawn because we are really interested in evaluating σ_w^2 rather than σ_e^2. Since the quantization noise sources are assumed to be white and uncorrelated, the average mean squared error is therefore given by:

$$\begin{aligned} \mathcal{E} &= \frac{c}{M} \sum_{k=0}^{M-1} 2^{-2b_k} \sigma_{y_k}^2 \int_{-\pi}^{\pi} \frac{|\tilde{R}_k(e^{j\omega})|^2}{|V_k(e^{j\omega})|^2} \frac{d\omega}{2\pi} \\ &= \frac{c}{M} \sum_{k=0}^{M-1} 2^{-2b_k} \int_{-\pi}^{\pi} S_{yy}(e^{j\omega})|R_k(e^{j\omega})|^2|V_k(e^{j\omega})|^2 \frac{d\omega}{2\pi} \int_{-\pi}^{\pi} \frac{|\tilde{R}_k(e^{j\omega})|^2}{|V_k(e^{j\omega})|^2} \frac{d\omega}{2\pi} \end{aligned} \tag{42}$$

Using the AM-GM inequality, equation (39) and the fact that $|R_k(e^{j\omega})|^2 = |\tilde{R}_k(e^{j\omega})|^2$, equation (42) reduces to:

$$\mathcal{E} \geq c2^{-2b}(\prod_{i=0}^{M-1} \int_{-\pi}^{\pi} S_{yy}(e^{j\omega})|V_k(e^{j\omega})|^2|\tilde{R}_k(e^{j\omega})|^2 \frac{d\omega}{2\pi} \int_{-\pi}^{\pi} \frac{|\tilde{R}_k(e^{j\omega})|^2}{|V_k(e^{j\omega})|^2} \frac{d\omega}{2\pi})^{1/M} \tag{43}$$

Applying the Cauchy-Schwartz inequality to each term in (43), we get:

$$\mathcal{E}_{min} = c2^{-2b}(\prod_{k=0}^{M-1} \int_{-\pi}^{\pi} \sqrt{S_{yy}(e^{j\omega})}|\tilde{R}_k(e^{j\omega})|^2 \frac{d\omega}{2\pi})^{2/M} \tag{44}$$

This minimum bound is achieved by choosing $|V_{opt}(e^{j\omega})|^2$ as in (40). Finally, (41) follows immediately from the definition of the coding gain, equation (7) and the fact that $\sigma_x^2 = \sigma_y^2/M$. ∎

The LTI case is indeed a loss of generality. Since the class of $(LPTV)_M$ filters and $(PTV)_M$ quantizers include the LTI case, it is clear that the performance of this more general class of filters and quantizers is at least as good as the LTI one. We have already shown that the optimum $(LPTV)_M$ filter for Fig. 9 reduces to a LTI one. The question then becomes : Is the $(PTV)_M$ quantizer providing any excess gain over the LTI case and if so, by how much ? We show next that, even in this restricted form of $(LPTV)_M$ filters, the coding gain of the above scheme is always greater than the LTI one except when the magnitude squared response of the polyphase components $R_k(e^{j\omega})$ of $F(e^{j\omega})$ are equal for all k. Starting from the denominator of (22) (the coding

gain expression of Fig. 6), one can write the following series of steps:

$$\begin{aligned}\frac{1}{M}(\int_{-\pi}^{\pi}\sqrt{S_{yy}(e^{j\omega})}\frac{d\omega}{2\pi})^2 &= \frac{1}{M}(\int_{-\pi}^{\pi}\sqrt{S_{yy}(e^{j\omega})}\sum_{k=0}^{M-1}|\tilde{R}_k(e^{j\omega})|^2\frac{d\omega}{2\pi})^2 \\ &= \frac{1}{M}(\sum_{k=0}^{M-1}\int_{-\pi}^{\pi}\sqrt{S_{yy}(e^{j\omega})}|\tilde{R}_k(e^{j\omega})|^2\frac{d\omega}{2\pi})^2 \\ &\geq \frac{1}{M}\times M^2((\prod_{i=0}^{M-1}\int_{-\pi}^{\pi}\sqrt{S_{yy}(e^{j\omega})}|\tilde{R}_k(e^{j\omega})|^2\frac{d\omega}{2\pi})^{1/M})^2 \\ &= M(\prod_{i=0}^{M-1}\int_{-\pi}^{\pi}\sqrt{S_{yy}(e^{j\omega})}|\tilde{R}_k(e^{j\omega})|^2\frac{d\omega}{2\pi})^{2/M}\end{aligned} \tag{45}$$

where the last line in (45) is the denominator of (41). Since the numerator is the same in both cases, the claim is proved. The first equality in (45) is obtained by using the power complementary property of the polyphase components of $F(e^{j\omega})$. The second line is a consequence of the linearity of the integral. The third line results from applying the AM-GM inequality. From the AM-GM formula, we know that equality is achieved if and only if all $|\tilde{R}_k(e^{j\omega})|^2$ are equal. From Fig. 22 (which was introduced in the proof of Theorem 7.1.1), we can see that this makes perfect sense. If all $|\tilde{R}_k(e^{j\omega})|^2$ are equal and since the optimum filters $V_k(e^{j\omega})$ are independent of k, the variance of the subband quantizer inputs will be all equal. There is therefore no variance disparity in the subbands and optimum bit allocation of the subband quantizers (which depends on the AM-GM inequality) can not produce any gain. Using the single band result, we can now derive closed form expressions for the optimum $V_{opt_k}(e^{j\omega})$ and the average minimum mean squared error for the multiband case.

Theorem 8.1.2. *Consider the scheme of Fig. 21 under the above assumptions. The optimum filter $V_{opt_k}(e^{j\omega})$ (for each k) that minimizes the average mean square reconstruction error at the output has the following magnitude squared response:*

$$|V_{opt_k}(e^{j\omega})|^2 = \frac{\sqrt{\sum_{i=0}^{L-1}|\tilde{R}_{ik}(e^{j\omega})|^2}}{\sqrt{S_k(e^{j\omega})}} \tag{46}$$

where $\tilde{R}_{ik}(e^{j\omega})$ is the kth polyphase component of the ith filter $\tilde{F}_i(e^{j\omega})$ and $S_k(e^{j\omega}) = \sum_{i=0}^{L-1} S_{y_i}(e^{j\omega})|\tilde{R}_{ik}(e^{j\omega})|^2$ is the power spectrum of kth channel. Using the above optimum filters, the coding gain of Fig. 21 is then given by :

$$\mathcal{G}_{opt} = \frac{\sigma_y^2}{M(\prod_{k=0}^{M-1}\int_{-\pi}^{\pi}\sqrt{S_k(e^{j\omega})}\sqrt{\sum_{i=0}^{L-1}|\tilde{R}_{ik}(e^{j\omega})|^2}\frac{d\omega}{2\pi})^{2/M}} \tag{47}$$

Proof. By interpreting the single band result as one of the L channels of the multiband model and by using result 2 of section III, the average mean squared error can be expressed as follows:

$$\begin{aligned}\mathcal{E} &= \frac{c}{M}\sum_{k=0}^{M-1}2^{-2b_k}\sigma_{y_k}^2\int_{-\pi}^{\pi}\frac{\sum_{i=0}^{L-1}|\tilde{R}_{ik}(e^{j\omega})|^2}{|V_k(e^{j\omega})|^2}\frac{d\omega}{2\pi} \\ &= \frac{c}{M}\sum_{k=0}^{M-1}2^{-2b_k}\int_{-\pi}^{\pi}S_k(e^{j\omega})|V_k(e^{j\omega})|^2\frac{d\omega}{2\pi}\int_{-\pi}^{\pi}\frac{\sum_{i=0}^{L-1}|\tilde{R}_{ik}(e^{j\omega})|^2}{|V_k(e^{j\omega})|^2}\frac{d\omega}{2\pi}\end{aligned} \tag{48}$$

Using the same inequalities as in the proof of theorem 8.1.1, we can immediately derive (46) and (47). ■

Following the same type of reasoning as before, we again expect the coding gain of the more general $(LPTV)_M$ case of Fig. 21 to be higher than the analogous LTI one of Fig. 17. However, the complexity of the expressions (25) and (47) in this case prevents a formal mathematical proof.

Example 8.1. *Equal polyphase components.* Assume that the input $x(n)$ is modeled as in Fig. 1 where the upsampler $M = 2$ and the driving input $y(n)$ is a zero mean gaussian AR(1) process with correlation coefficient $0 < \rho < 1$. Furthermore, let $F(z)$ be the optimum FIR compaction filter of length two given by $\frac{1}{\sqrt{2}}(1 + z^{-1})$. The filter actually corresponds to one of the channels of a 2×2 KLT which is independent of the input statistics. In this case, the polyphase components of $F(e^{j\omega})$ are $R_0(e^{j\omega}) = R_1(e^{j\omega}) = \frac{1}{\sqrt{2}}$. Substituting in (41) and simplifying, we get (21), the coding gain expression of Fig. 6. In example 7.2., a closed form expression was derived for the AR(1) case and a plot of the coding gain is shown in Fig. 20.

Example 8.2. *Unequal polyphase components.* With the same set of assumptions of example 8.1, let the filter $F(z)$ be the optimum FIR compaction filter of length four. With $M = 2$ and assuming an AR(1) process, the following closed form expression was derived in [18] for the optimum compaction filter:

$$F(z) = a + cz^{-1} + bz^{-2} + dz^{-3} \tag{49}$$

where

$$a = \frac{1}{p\sqrt{2}}\sqrt{\sqrt{p} + \sqrt{q}}\ ,\ b = \frac{1}{p\sqrt{2}}(\sqrt{\sqrt{p} + \sqrt{q}} - \sqrt{p}\sqrt{\sqrt{p} - \sqrt{q}})$$
$$c = \frac{1}{p\sqrt{2}}(\sqrt{p}\sqrt{\sqrt{p} + \sqrt{q}} - \sqrt{\sqrt{p} - \sqrt{q}}\ ,\ d = -\frac{1}{p\sqrt{2}}\sqrt{\sqrt{p} - \sqrt{q}}$$

and $p = 3 + \rho^2$, $q = 2 + \rho^2$. The polyphase components of $F(e^{j\omega})$ are $R_0(e^{j\omega}) = a + be^{-j\omega}$ and $R_1(e^{j\omega}) = c + de^{-j\omega}$. Substituting the power spectrum expression of an AR(1) process given by (36) into (41) and using some useful integral formulas (see [17] pp. 429), we can derive the following coding gain expression for the scheme of Fig. 9:

$$\mathcal{G}_{opt} = \frac{1}{2(1-\rho^2)\frac{2}{\pi}((a^2 + b^2 + \frac{2ab}{\rho})K(\rho) - \frac{2ab}{\rho}E(\rho))\frac{2}{\pi}((c^2 + d^2 + \frac{2cd}{\rho})K(\rho) - \frac{2cd}{\rho}E(\rho))} \tag{50}$$

where K(.) is the complete elliptic integral of the first kind and E(.) is the complete elliptic integral of the second kind. There is a reason for writing the denominator of (50) in this form. It can be shown that the factors $\frac{2}{\pi}((a^2 + b^2 + \frac{2ab}{\rho})\ K(\rho) - \frac{2ab}{\rho}E(\rho))$ and $\frac{2}{\pi}((c^2 + d^2 + \frac{2cd}{\rho})K(\rho) - \frac{2cd}{\rho}E(\rho))$ represent the variance of the outputs $R_0(e^{j\omega})$ and $R_1(e^{j\omega})$ respectively (with an input with power spectrum $\sqrt{S_{yy}(e^{j\omega})}$). Their product is the geometric mean which produces the extra gain over the LTI case. The further away they are in magnitude, the more gain we will obtain. The plots of the coding gain formulas (37) and (50) are shown in Fig. 23. We notice that the coding gain of the $(LPTV)_M$ case is indeed greater than the LTI one for all values of ρ, although not by a substantial amount for the AR(1) $y(n)$.

8.2. Using an orthonormal filter bank

Consider now the M-channel orthonormal filter bank shown in Fig. 10 for the single band model and in Fig. 24 for the multiband model. As in the previous subsection, we first analyze the single band case in detail and

then use the corresponding results to derive analogous expressions for the multiband case. The quantization noise assumptions of the previous subsection are still true here. The goal is again to jointly allocate the subband bits b_k under the constraint (39) and optimize the orthonormal filter bank in order to minimize the average m.s.e.

Theorem 8.2.1. *Consider the scheme of Fig. 10 under the above assumptions. The synthesis section of the optimum orthonormal filter bank* $\{P_k(e^{j\omega})\}$ *corresponds to choosing one of the filters, say* $\tilde{P}_0(e^{j\omega})$ *to be equal to* $\tilde{F}(e^{j\omega})$ *and the remaining filters* $\tilde{P}_k(e^{j\omega})$, $k = 1, \ldots, M-1$, *to be orthogonal to* $\tilde{P}_0(e^{j\omega})$. *In this case, the optimum orthonormal filter bank reduces to Fig. 5 where the quantizer* Q *is allocated* Mb *bits according to (37).*

Proof. By applying the blocking operation and using the polyphase representation [5], the scheme of Fig. 10 can be redrawn as in Fig. 25, where $\mathbf{E}(e^{j\omega})$ is the polyphase matrix of the analysis bank, $\mathbf{E}^\dagger(e^{j\omega})$ is the polyphase matrix of the synthesis bank and $\tilde{R}_k(e^{j\omega})$, $k = 0, \ldots, M-1$, are the M polyphase components of the filter $\tilde{F}(e^{j\omega})$. Let $\mathbf{U}(e^{j\omega})$ be the $1 \times M$ vector whose kth element is $\tilde{R}_k(e^{j\omega})$. Then, the average m.s.e can be expressed as follows:

$$\mathcal{E} = \frac{1}{M} \int_{-\pi}^{\pi} trace(\mathbf{U}(e^{j\omega})\mathbf{E}(e^{j\omega})\mathbf{S_{qq}}\mathbf{E}^\dagger(e^{j\omega})\mathbf{U}^\dagger(e^{j\omega})) \frac{d\omega}{2\pi} \tag{51}$$

Since the integrand is in a quadratic form, the trace operator can be removed. Furthermore, since $\mathbf{E}(e^{j\omega})\mathbf{E}^\dagger(e^{j\omega}) = I$ by orthonormality and $\mathbf{U}(e^{j\omega})\mathbf{U}^\dagger(e^{j\omega})) = 1$ by the Nyquist property of the $F(e^{j\omega})$, we can rewrite (51) as follows:

$$\mathcal{E} = \frac{1}{M} \int_{-\pi}^{\pi} \frac{\mathbf{P}(e^{j\omega})\mathbf{S_{qq}}\mathbf{P}^\dagger(e^{j\omega})}{\mathbf{P}(e^{j\omega})\mathbf{P}^\dagger(e^{j\omega})} \frac{d\omega}{2\pi} \tag{52}$$

where $\mathbf{P}(e^{j\omega}) = \mathbf{U}(e^{j\omega})\mathbf{E}(e^{j\omega})$. Since the integrand of (52) is positive for all ω, minimizing (52) is equivalent to minimizing the integrand at each frequency. But for any fixed frequency ω_0, the ratio $\frac{\mathbf{P}(e^{j\omega_0})\mathbf{S_{qq}}\mathbf{P}^\dagger(e^{j\omega_0})}{\mathbf{P}(e^{j\omega_0})\mathbf{P}^\dagger(e^{j\omega_0})}$ is a Rayleigh quotient. For each frequency ω, the minimizing vector $\mathbf{P}_{opt}(e^{j\omega})$ has the form $(0 \ \ldots \ 1 \ \ldots \ 0)$ where the 1 in the ith position corresponds to the minimum noise variance $\sigma^2_{q_i}$. Since $\mathbf{P}(e^{j\omega}) = \mathbf{U}(e^{j\omega})\mathbf{E}(e^{j\omega})$, the minimizing vector $\mathbf{P}_{opt}(e^{j\omega})$ can be obtained by setting the ith column in $\mathbf{E}(e^{j\omega})$ to be equal to $\mathbf{U}^\dagger(e^{j\omega})$ and all the remaining columns to be orthogonal to $\mathbf{U}(e^{j\omega})$. This is equivalent to the statement of the theorem. ■

The optimum orthonormal filter bank thus reduces to the scheme of Fig. 5 with Mb bits allocated to the quantizer. The result of Theorem 8.2.1 is very intuitive and somehow expected: filter and decimate the oversampled signal $x(n)$ according to its model and then quantize $y(n)$ in Fig. 5 with $\hat{b} = Mb$ bits per sample. As we mentioned before, this amounts to fixing the bit rate (number of bits per second) in order to trade quantization resolution with sampling rate. It is interesting though to see that this very intuitive scheme is equivalent to using an optimum orthonormal filter bank as a sophisticated quantizer to the input $x(n)$. With (7) in mind, the coding gain expression can be derived following the lines of the proof of Theorem 5.1 and is equal to $2^{2b(M-1)}$. This is an exponential gain which can be quite large for moderate values of M but unlike all previous schemes, depends on the bit rate b. Finally, to end this section, we would like to derive an analogous result (to Theorem 8.2.1) for the multiband case.

Theorem 8.2.2. *Consider the scheme of Fig. 24 under the same assumptions. The synthesis section of the optimum orthonormal filter bank corresponds to choosing L of the filters to be equal to $\tilde{F}_k(e^{j\omega})$ and the remaining filters $Q_k(e^{j\omega})$, $k = L+1, \ldots, M-1$, to be the $M-L-1$ orthogonal filters to $F_i(e^{j\omega})$, $i = 0, \ldots, L-1$. In this case, the optimum orthonormal filter bank reduces to Fig. 16 with an equivalent average number of bits $\hat{b}$ equal to Mb/L bits.*

Proof. By interpreting the single band result as one of the L channels of the multiband model and by using result 2 and equation (39), the result follows immediately. ∎

With the above $\hat{b}$, we can now perform an optimum allocation of subband bits for the scheme of Fig. 16. This is a standard allocation problem that arises in subband coding application [11]. By applying the AM-GM inequality to the output error expression $\mathcal{E} = c\frac{1}{M}\sum_{k=0}^{L-1} 2^{-2b_k}\sigma_{y_k}^2$, we get

$$\mathcal{E}_{min} = c2^{-2b\frac{M}{L}}\frac{L}{M}\left(\prod_{i=0}^{L-1}\sigma_{y_i}^2\right)^{1/M} \tag{53}$$

which can be achieved by setting $b_k = b + 0.5\log_2\sigma_{y_k}^2 - 0.5\log_2\prod_{i=0}^{L-1}(\sigma_{y_i}^2)^{1/M}$. This optimum bit allocation formula will in almost all cases yield non integer solution for the bits. A quick remedy might be to use a simple rounding procedure or a more sophisticated algorithm [19] to obtain integer solutions. A detailed discussion of the topic of allocating *integer* bits to the channel quantizers is however outside the scope of the paper. The noise variance in Fig. 12 simplifies to $c2^{-2b}\frac{L}{M}\left(\frac{1}{L}\sum_{k=0}^{L-1}\sigma_{y_k}^2\right)$. The coding gain expression takes therefore the following form:

$$\mathcal{G}_{opt} = 2^{2b(\frac{M}{L}-1)}\frac{AM(\sigma_{y_i}^2)}{GM(\sigma_{y_i}^2)} \tag{54}$$

where AM is the arithmetic mean, GM is the geometric mean and $\sigma_{y_i}^2$ is the variance of the ith signal $y_i(n)$ in Fig. 2. We observe that when $L = 1$, we get the coding gain of the single band case and when $L = M$, the scheme of Fig. 16 reduces to an orthonormal filter bank, the average number of bits is equal to b and (54) reduces to the well known expression of the coding gain of an orthonormal filter bank.

Appendix A.

Proof of result 1 *in section III.* The interpolated subband signals can be expressed as $x_i(n) = \sum_k y_i(k)f_i(n-Mk)$. Hence,

$$E[x_i(n)x_j^*(n-Mm)] = E\left[\sum_{k'} y_i(k')f_i(n-Mk')\sum_k y_j^*(k)f_j^*(n-Mk-Mm)\right] \tag{55}$$

Let $r(u)$ be the cross correlation between the jointly WSS processes $y_i(n)$ and $y_j(n)$, that is, $r(u) = E[y_i(n)y_j^*(n-u)$. Using the change of variable $k'-k = l$, the preceding equation becomes:

$$E[x_i(n)x_j^*(n-Mm)] = \sum_l r(l)\sum_{k'} f_i(n-Mk')f_j^*(n+M(l-m)-Mk') \tag{56}$$

Substituting (56) in the left hand side of (3), we get:

$$\frac{1}{M}\sum_{l} r(l) \sum_{k'} \sum_{k=0}^{M-1} f_i(n-(Mk'+k)) {f_j}^*(n+M(l-m)-(Mk'+k)) \tag{57}$$

Since M is positive, k' and k are integers and $0 \leq k < M$, we can always replace $Mk'+k$ by an integer u. That is, there always exist an integer u such that k' is the quotient and k is the remainder obtained from dividing u by M. We can therefore rewrite (57) as follows:

$$\frac{1}{M}\sum_{l} r(l) \sum_{u} f_i(n-u) {f_j}^*(n+M(l-m)-u) = \frac{1}{M}\sum_{l} r(l) \sum_{k} f_i(k) {f_j}^*(k+M(l-m)) \tag{58}$$

But the orthonormality of the filter bank implies, in particular, that $\sum_{k} f_i(k) {f_j}^*(k+M(l-m)) = 0 \quad \forall\, l,m.$ Thus, the inner sum in (58) reduces to zero and the result follows. ■

Appendix B.

Phase randomization of a $(CWSS)_M$ process. A WSS process $\hat{x}(n)$ can be obtained from a $(CWSS)_M$ process $x(n)$ by introducing a random shift θ in the $(CWSS)_M$ signal $x(n)$ [12],[13],[14]. The parameter θ is a discrete random variable that can take any integer value from 0 to $M-1$ with equal probability $1/M$. Furthermore, the random variable θ is assumed to be independent of $x(n)$. The autocorrelation function of $\hat{x}(n)$ is given by:

$$\begin{aligned} R_{\hat{x}\hat{x}}(n,k) &= E\{\hat{x}(n)\hat{x}(n-k)\} = E_\theta\{E\{x(n-\theta)x(n-k-\theta)|\theta\}\} = E_\theta\{R_{yy}(n-\theta,k)\} \\ &= \sum_{\theta=-\infty}^{\infty} R_{xx}(n-\theta,k)p(\theta) = \frac{1}{M}\sum_{\theta=0}^{M-1} R_{xx}(n-\theta,k) = \frac{1}{M}\sum_{m=n}^{M+n-1} R_{xx}(m,k) \end{aligned} \tag{59}$$

Now observe that

$$\begin{aligned} \frac{1}{M}\sum_{m=n}^{M+n-1} R_{xx}(m,k) &= \frac{1}{M}\sum_{m=0}^{M-1} R_{xx}(m,k) + \frac{1}{M}\sum_{m=M}^{M+n-1} R_{xx}(m,k) - \frac{1}{M}\sum_{m=0}^{n-1} R_{xx}(m,k) \\ &= \frac{1}{M}\sum_{m=0}^{M-1} R_{xx}(m,k) + \frac{1}{M}\sum_{m=M}^{M+n-1} R_{xx}(m,k) - \frac{1}{M}\sum_{m=M}^{M+n-1} R_{xx}(m,k) \\ &= \frac{1}{M}\sum_{m=0}^{M-1} R_{xx}(m,k) \end{aligned} \tag{60}$$

The second line follows because $R_{xx}(m,k) = R_{xx}(m+M,k)$ by cyclostationarity. The last sum is independent of n implying that $R_{\hat{x}\hat{x}}(n,k)$ is a function of k only and that the process $\hat{x}(n)$ is indeed WSS. Furthermore,

$$\hat{R}_{xx}(k) = \frac{1}{M}\sum_{n=0}^{M-1} R_{xx}(n,k) \tag{61}$$

Appendix C.

Proof of equation (13). Let $x(n)$ be a $(CWSS)_M$ process input to a linear time invariant filter $P(e^{j\omega})$. The output $z(n)$ is a $(CWSS)_M$ process [8] and is related to $x(n)$ by the well known convolution sum $z(n) = \sum_i p(i)x(n-i)$.

Our goal is to derive an expression for the average variance of the $(CWSS)_M$ process $z(n)$. So,

$$\begin{aligned}\sigma_z^2 &= \frac{1}{M}\sum_{n=0}^{M-1} E\{|z(n)|^2\} = \frac{1}{M}\sum_{n=0}^{M-1}\sum_i\sum_j p(i)p^*(j)E\{x(n-i)x^*(n-j)\} \\ &= \sum_i\sum_j p(i)p^*(j)\frac{1}{M}\sum_{n=0}^{M-1} R_{xx}(n,j-i) = \sum_i\sum_j p(i)p^*(j)\hat{R}_{xx}(j-i)\end{aligned} \tag{62}$$

where the last equality follows from equation (61). By making the change of variables $j-i=l$, we get :

$$\sigma_z^2 = \sum_l\sum_j p(j-l)p^*(j)\hat{R}_{xx}(l) = \sum_l\sum_l r_p(l)\hat{R}_{xx}(l) \tag{63}$$

where $r_p(l) \triangleq \sum_k p^*(k)p(k-n)$ is the deterministic autocorrelation of $p(n)$. Taking the discrete time fourier transform of (63), we get (11). ■

Appendix D.

Power spectral density of an interpolated random process. Let $y(n)$ be a wide sense stationary (WSS) random process, input to an interpolation filter as shown in Fig. 1. The output $x(n)$ is in general a $(CWSS)_M$ process [8]. The average power spectral density of the "stationarized" process has the form

$$\hat{S}_{xx}(e^{j\omega}) = \frac{1}{M}S_{yy}(e^{j\omega M})|F(e^{j\omega})|^2 \tag{64}$$

To derive (64), we can use (61) to write

$$\hat{R}_{xx}(k) = \frac{1}{M}\sum_i\sum_j R_{yy}(i-j)\sum_{n=0}^{M-1} f(n-Mi)f(n-k-Mj) \tag{65}$$

Making the consecutive change of variables $i-j=l$ and $n-Mi=u$, equation (65) simplifies to:

$$\begin{aligned}\hat{R}_{xx}(k) &= \frac{1}{M}\sum_l R_{yy}(l)\sum_i\sum_{u=-Mi}^{M-1-Mi} f(u)f(u-k+Ml) \\ &= \frac{1}{M}\sum_l R_{yy}(l)\sum_u f(u)f(u-(k-Ml)) = \frac{1}{M}\sum_l R_{yy}(l)r_f(k-Ml)\end{aligned} \tag{66}$$

where $r_f(n)$ is the deterministic autocorrelation of $f(n)$ as defined in appendix C. Equation (66) can be interpreted as passing the autocorrelation sequence $\frac{1}{M}R_{yy}(n)$ through the interpolation filter $r_f(n)$. Taking the fourier transform of (66), we obtain (64) or equivalently (12). The expression for multiband case, equation (15), can be obtained in a similar fashion. Again, from (61), one can write:

$$\begin{aligned}\hat{R}_{xx}(k) &= \frac{1}{M}\sum_{n=0}^{M-1} E\{x(n)x^*(n-k)\} = \frac{1}{M}\sum_{n=0}^{M-1}\sum_i\sum_j \mathbf{f}(n-Mi)E\{\mathbf{y}(n)\mathbf{y}^\dagger(n-k)\}\mathbf{f}^\dagger(n-k-Mj) \\ &= \frac{1}{M}\sum_{n=0}^{M-1}\sum_i\sum_j \mathbf{f}(n-Mi)\mathbf{R}_\mathbf{y}(k)\mathbf{f}^\dagger(n-k-Mj)\end{aligned} \tag{67}$$

where $\mathbf{f}(n) = (\, f_0(n) \quad f_1(n) \quad \ldots \quad f_{L-1}(n)\,)^T$ and $\mathbf{R}_\mathbf{y}(k)$ is the autocorrelation matrix of the L WSS inputs $y_k(n)$. By following the same steps used to derive (64), we obtain (13). ■

REFERENCES

[1] Jerri, A.J., "The Shannon sampling theorem - its various extensions and applications: a tutorial review", Proc. IEEE, pp. 1565-1596, Nov. 1977.

[2] Walter, G.G., "A sampling theorem for wavelet subspaces", IEEE Trans. on Information Theory, pp. 881-884, March 1992.

[3] Vaidyanathan, P.P. and Phoong, S., "Reconstruction of sequences from non uniform samples", ISCAS Proc., pp. 601-604, Seattle 1995.

[4] Vaidyanathan, P.P. and Phoong, S., "Discrete time signals which can be recovered from samples", ICASSP Proc., pp. 1448-1451, Detroit 1995.

[5] Vaidyanathan, P.P., *Multirate systems and filter banks,* Prentice Hall, Inc., Englewood Cliffs, 1993.

[6] Aziz, P., Sorensen, H. and Van Der Spiegel, J., "An overview of sigma-delta converters", IEEE Signal Processing Magazine, vol. 13, No. 1, pp. 61-84, January 1996.

[7] Gladyshev, E.G., "Periodically correlated random sequences", Soviet Mathematics, Vol. 2, pp.385-388, 1961.

[8] Sathe, V.S. and Vaidyanathan, P.P., "Effects of multirate systems on the statistical properties of random signals", IEEE Trans. on Signal Processing, pp. 131-146, Vol. 41, January 1993.

[9] Tsatsanis, M.K. and Giannakis, G.B.,"Principal component filter banks for optimal multiresolution analysis", IEEE Trans. on Signal Processing, pp. 1766-1777, Vol. 43, August 1995.

[10] Unser, M.,"On the optimality of ideal filters for pyramid and wavelet signal approximation", IEEE Trans. on Signal Processing, pp. 3591-3596, December 1993.

[11] Jayant, N.S. and Noll, P. *Digital coding of waveforms,* Prentice Hall, Inc., Englewood Cliffs, New Jersey, 1984.

[12] Gardner, W.A., "Stationarizable random processes", IEEE Trans. on Information Theory, vol. 24, No. 1, pp. 8-22, January 1978.

[13] Hurd, H.L., "Stationarizing properties of random shifts", SIAM Journal of Applied Mathematics, Vol. 26, No. 1, pp. 203-212, January 1974.

[14] Gardner, W.A. and Franks, L.E., "Characterization of cyclostationary random processes", IEEE Trans. on Information Theory, vol. 21, No. 1, pp.4-14, January 1975.

[15] Gelfand, I.M. and Fomin, S.V. *Calculus of variations,* Prentice Hall, Inc., Englewood Cliffs, New Jersey, 1963.

[16] Tuqan, J. and Vaidyanathan, P.P., "Statistically optimum pre- and post filtering in quantization", to be published in the IEEE Trans. on Circuit and Systems II.

[17] Gradshteyn, I.S. and Ryzhik, I.M. *Table of integrals, series, and products,* fifth edition, Academic press Inc., San Diego, California, 1994.

[18] Kirac, A. and Vaidyanathan, P. P., "Theory and design of optimum FIR compaction filters", submitted to the IEEE Trans. on Signal Processing.

[19] Jain, A.K., *Fundamentals of digital image processing,* Prentice Hall, Inc., Englewood Cliffs, 1989.

LIST OF FIGURES

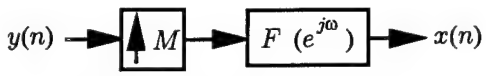

Fig. 1. The single band model .

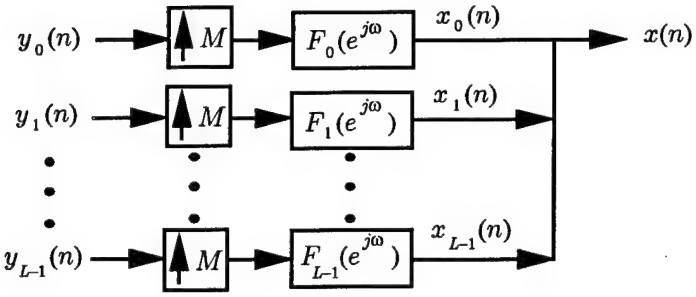

Fig. 2. The multiband model .

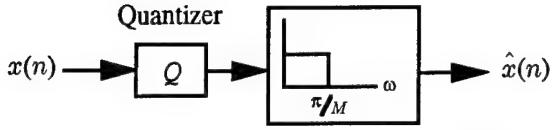

Fig. 3. Schematic of the oversampling PCM technique.

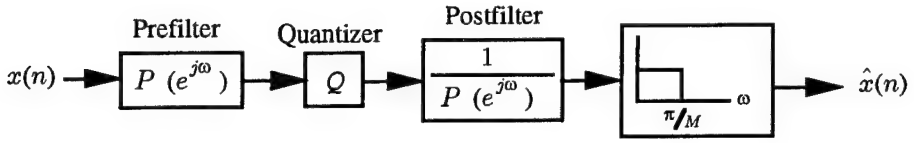

Fig. 4. The quantization scheme of Fig. 3 with noise shapers.

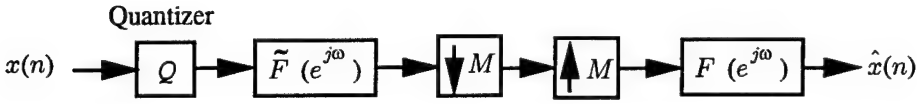

Fig. 5. Multirate quantization scheme for the single band case.

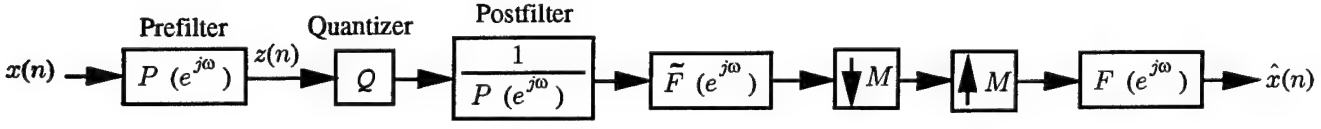

Fig. 6. Noise shaping by LTI pre- and post filters for the single band case where the postfilter is assumed to be the inverse of the prefilter.

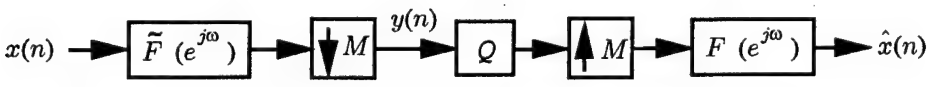

Fig. 7. Quantizing the lower rate signal $y(n)$ (single band case).

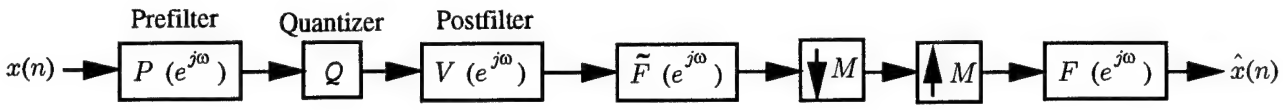

Fig. 8. General LTI pre- and post filters for noise shaping for the single band case.

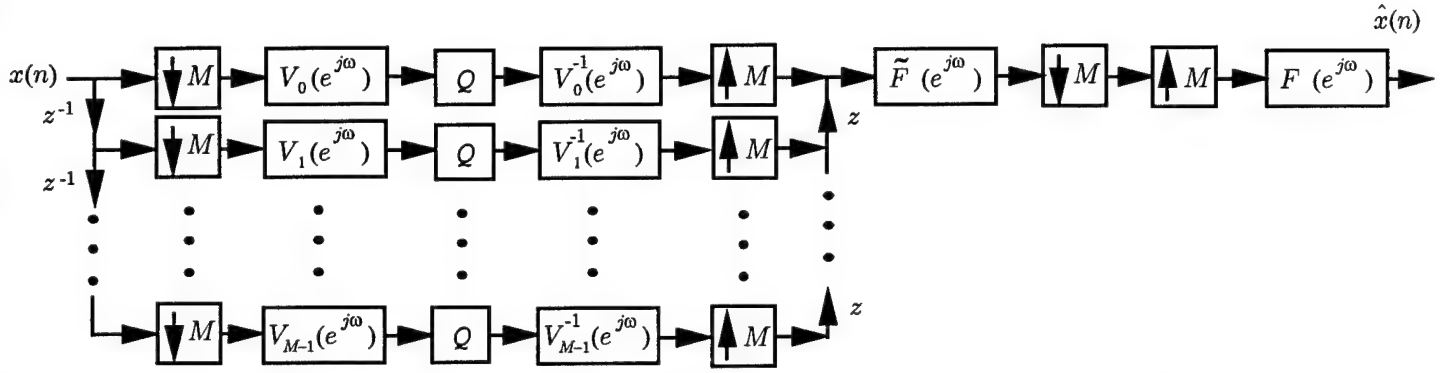

Fig. 9. Scheme 1 for noise shaping using $(LPTV)_M$ pre- and post filters (the single band case).

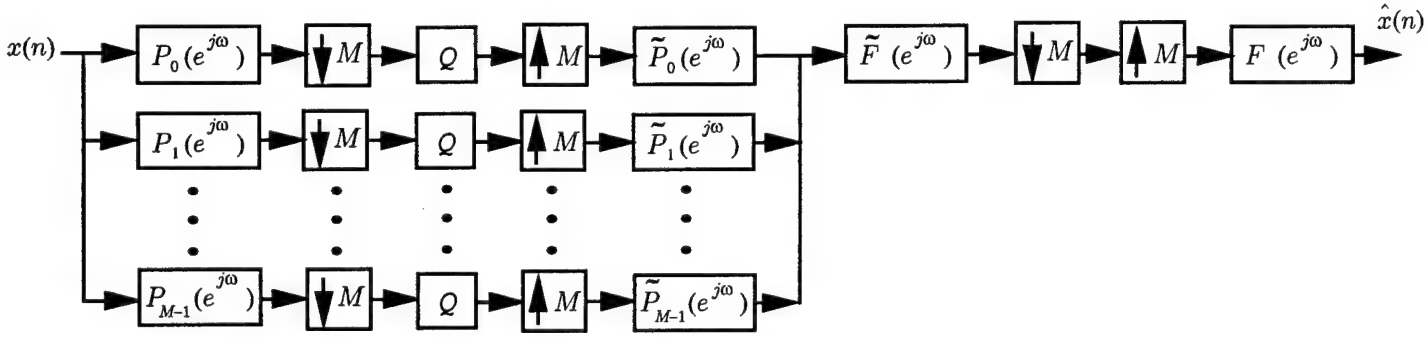

Fig. 10. Scheme 2 for noise shaping using $(LPTV)_M$ pre- and post filters (the single band case).

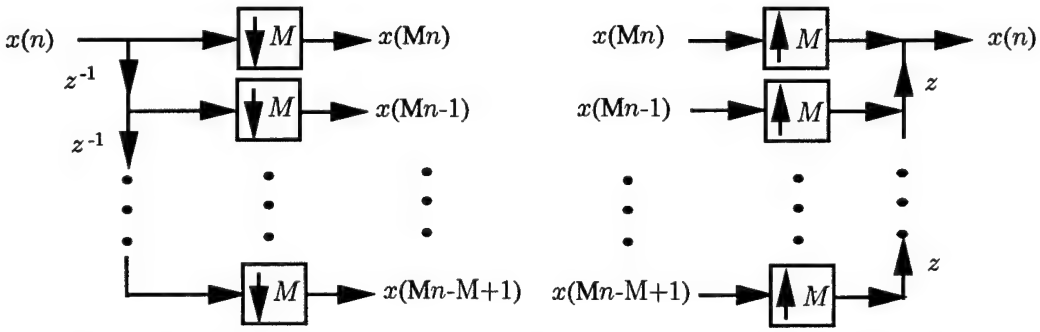

Fig. 11. M-fold blocking of a signal and unblocking of an M x 1 vector signal

Fig. 12. Direct quantization of $x(n)$.

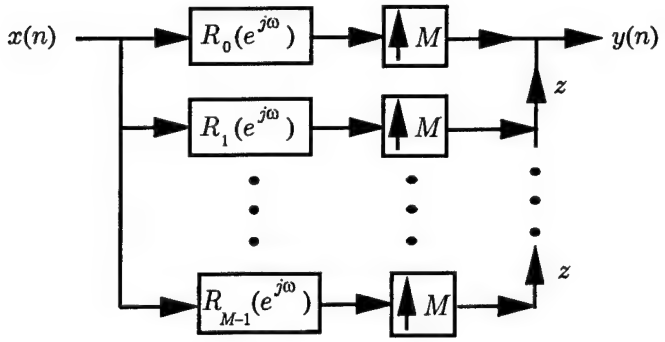

Fig. 13. The equivalent polyphase representation of Fig. 1.

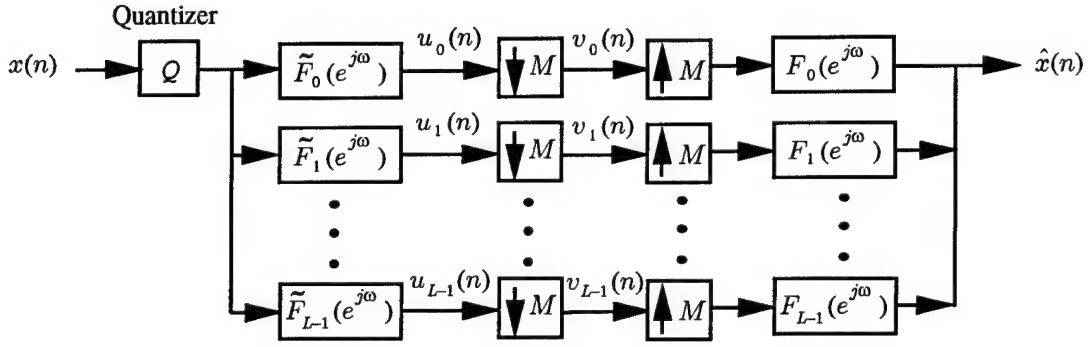

Fig. 14. Multirate quantization scheme for the multiband model.

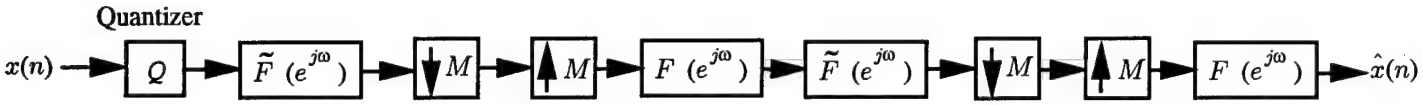

Fig. 15. A cascade of two multirate interconnections for the single band case.

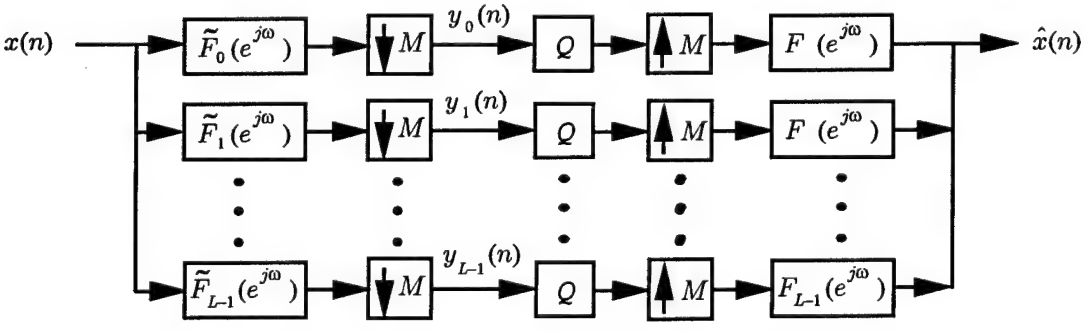

Fig. 16. Quantizing the lower rate signals $y_k(n)$ (multiband case).

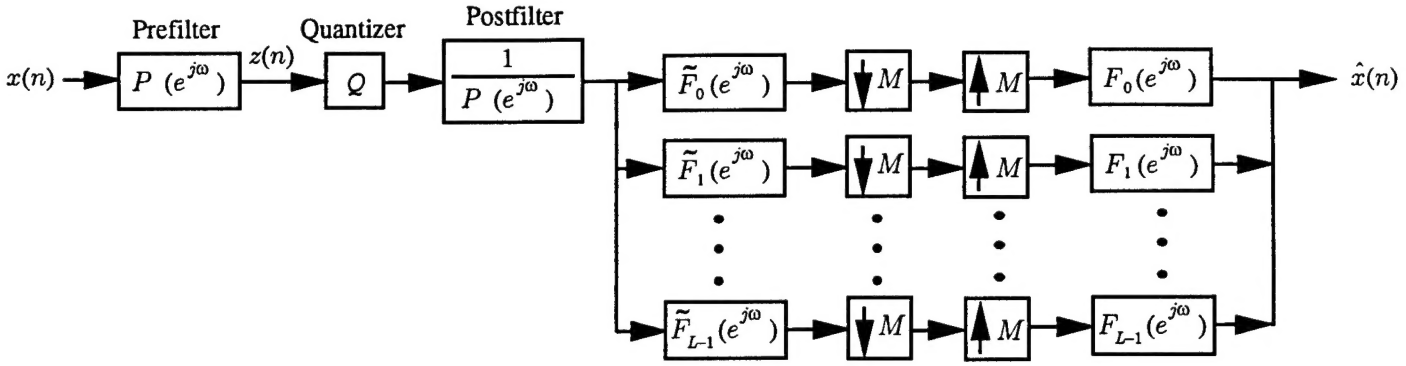

Fig. 17. Noise shaping by LTI pre- and post filters for the multiband case where the postfilter is assumed to be the inverse of the prefilter.

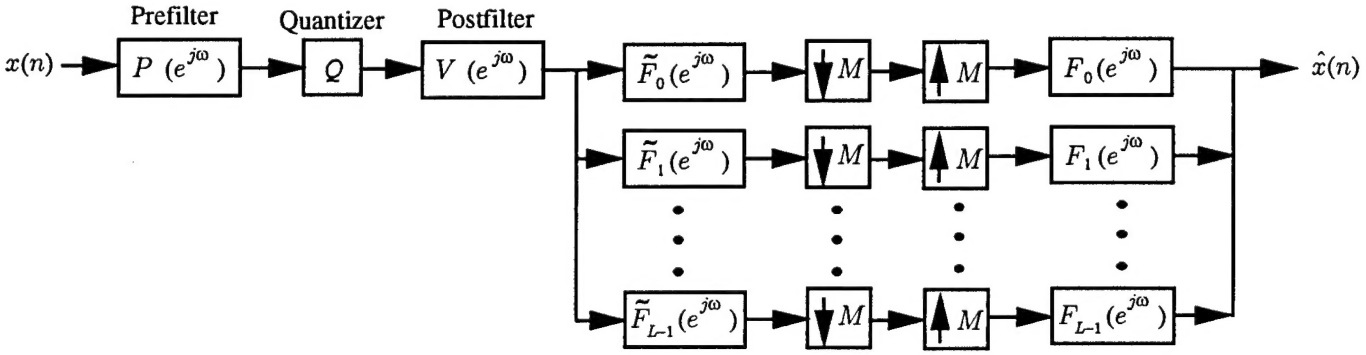

Fig. 18. General LTI pre- and post filters for noise shaping for the multiband case.

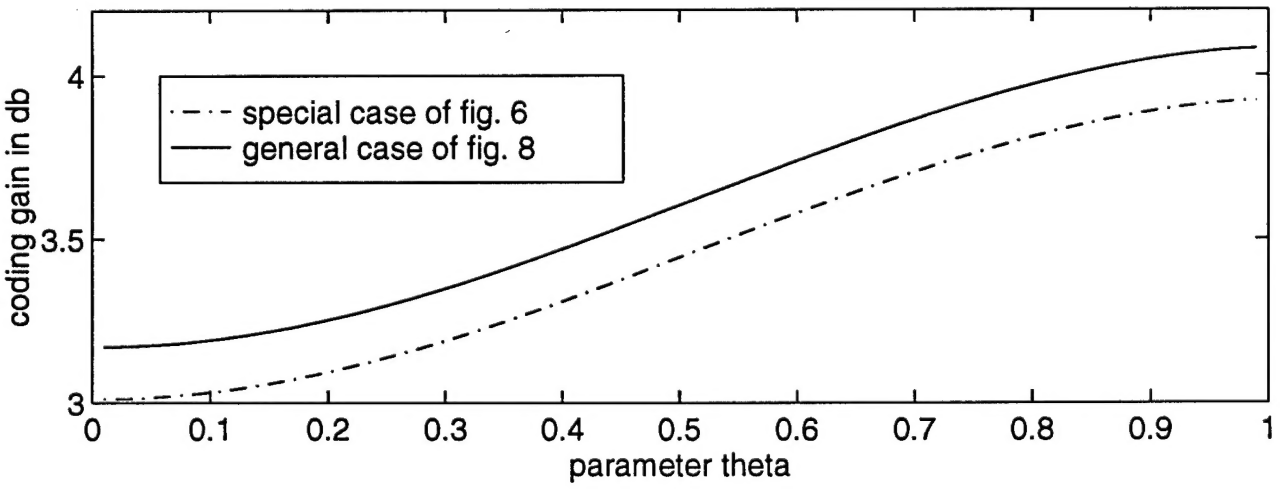

Fig. 19. Coding gain curves for the MA(1) case with $b = 3$ and $c = 2.4$.

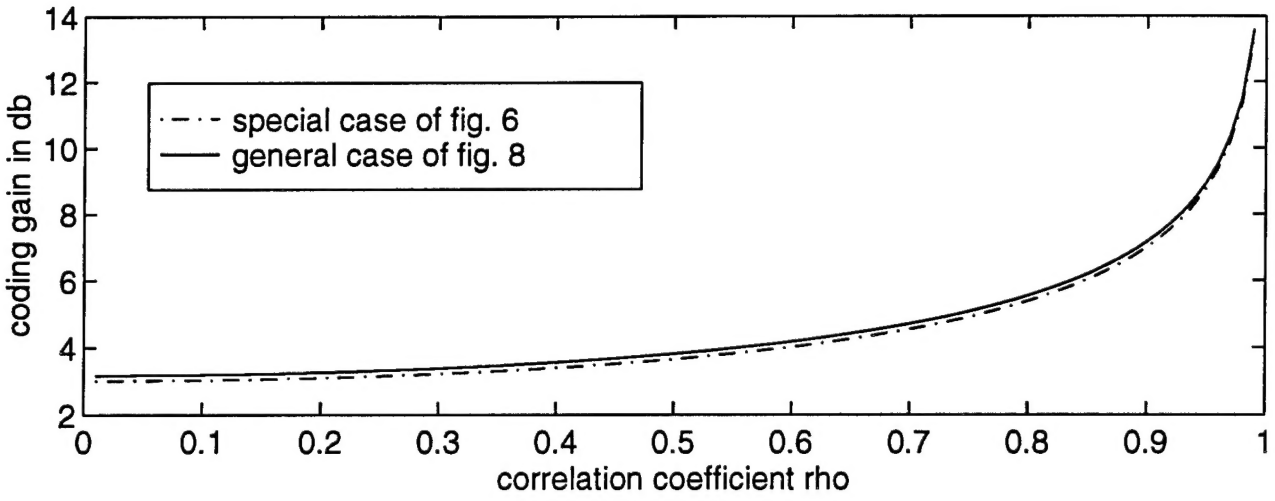

Fig. 20. Coding gain curves for the AR(1) case with $b = 3$ and $c = 2.4$.

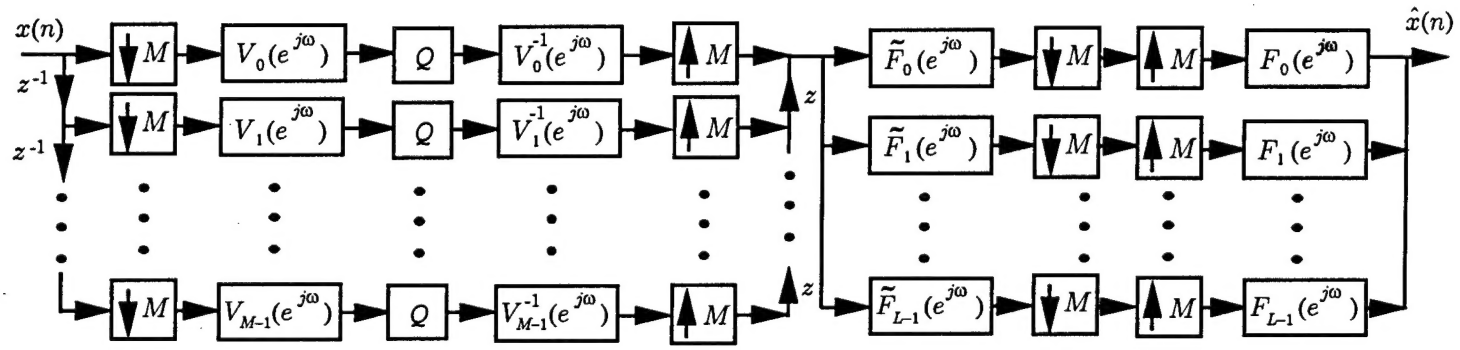

Fig. 21. Scheme 1 for noise shaping using $(LPTV)_M$ pre- and post filters (the multiband case).

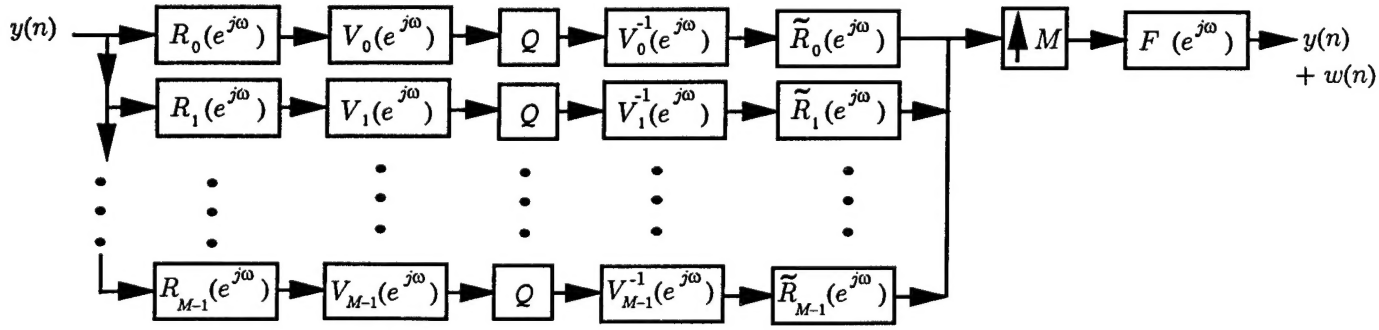

Fig. 22. An equivalent representation of Fig. 9.

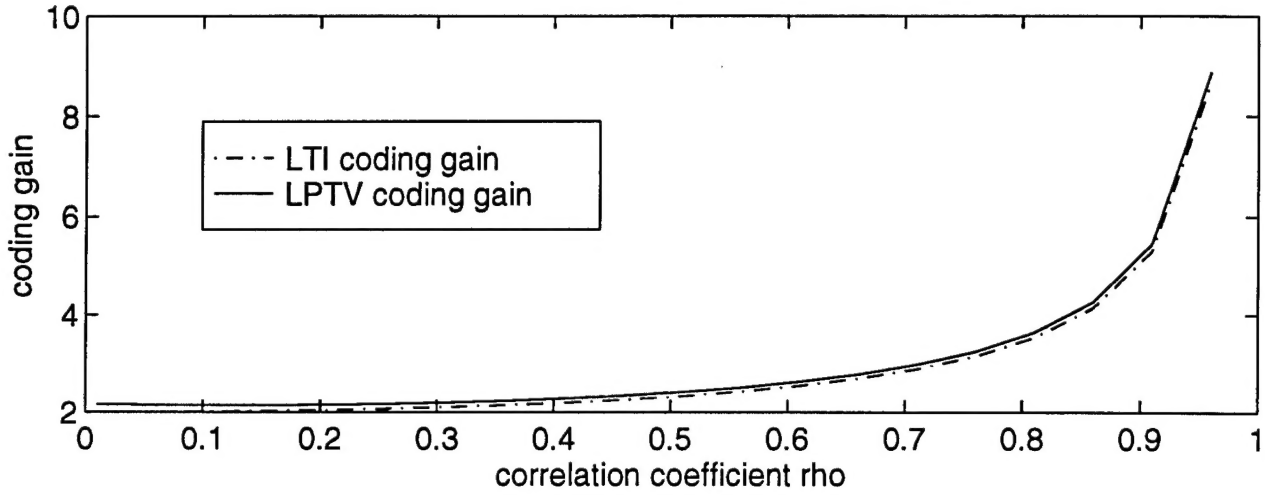

Fig. 23. Coding gain curves for the LTI and $(LPTV)_M$ cases under the assumption of a single band model with $M = 2$ and $y(n)$ is an AR(1) process.

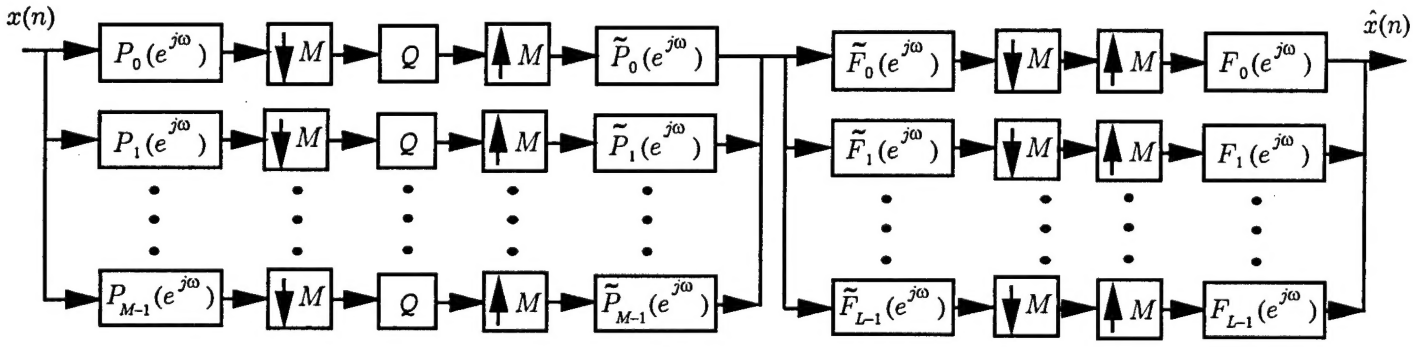

Fig. 24. Scheme 2 for noise shaping using $(LPTV)_M$ pre- and post filters (the multiband case).

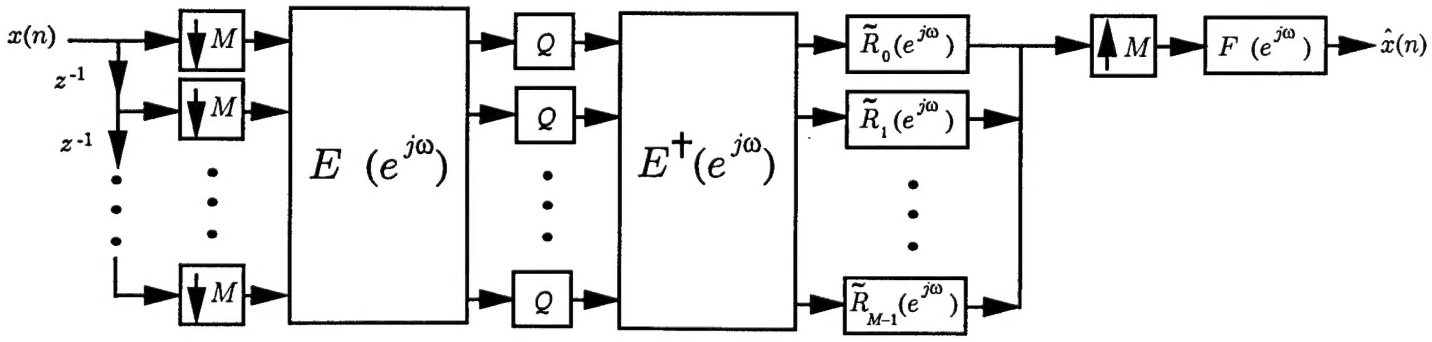

Fig 25. The polyphase representation of Fig. 10.

FOOTNOTES

1. Manuscript received _____

2. Work supported in parts by Office of Naval Research grant N00014-93-1-0231, Rockwell International and Tektronix, Inc.

3. The authors are with the Department of Electrical Engineering, California Institute of Technology, Pasadena, CA 91125.